Mathematical Models and Methods in Applied Sciences
(2022)

DOI: 10.1142/S021820252250052X

A stochastic model of grain boundary dynamics: A Fokker–Planck perspective

Yekaterina Epshteyn*
Department of Mathematics, The University of Utah,
Salt Lake City, UT 84112, USA
epshteyn@math.utah.edu

Chun Liu
Department of Applied Mathematics,
Illinois Institute of Technology,
Chicago, IL 60616, USA
cliu124@iit.edu

Masashi Mizuno
Department of Mathematics,
College of Science and Technology, Nihon University,
Tokyo 101-8308, Japan
mizuno.masashi@nihon-u.ac.jp

Received 27 June 2021
Revised 4 May 2022
Accepted 11 July 2022
Published 25 October 2022
Communicated by P. Degond

Many technologically useful materials are polycrystals composed of small monocrystalline grains that are separated by grain boundaries of crystallites with different lattice orientations. The energetics and connectivities of the grain boundaries play an essential role in defining the effective properties of materials across multiple scales. In this paper we derive a Fokker–Planck model for the evolution of the planar grain boundary network. The proposed model considers anisotropic grain boundary energy which depends on lattice misorientation and takes into account mobility of the triple junctions, as well as independent dynamics of the misorientations. We establish long time asymptotics of the Fokker–Planck solution, namely the joint probability density function of misorientations and triple junctions, and closely related the marginal probability density of misorientations. Moreover, for an equilibrium configuration of a boundary network, we derive explicit local algebraic relations, a generalized Herring Condition formula, as

*Corresponding author

well as formula that connects grain boundary energy density with the geometry of the grain boundaries that share a triple junction. Although the stochastic model neglects the explicit interactions and correlations among triple junctions, the considered specific form of the noise, under the fluctuation–dissipation assumption, provides partial information about evolution of a grain boundary network, and is consistent with presented results of extensive grain growth simulations.

Keywords: Grain growth; grain boundary network; texture development; lattice misorientation; triple junction drag; Fokker–Planck equation; fluctuation–dissipation theorem; weighted L^2 space; long time asymptotics; sharp-interface grain growth simulations.

AMS Subject Classification 2020: 74N15, 35R37, 35Q84, 35K15, 93E03, 53C21, 49Q20, 65M22

1. Introduction

Most technologically useful materials are polycrystalline microstructures composed of a myriad of small monocrystalline grains separated by grain boundaries. The energetics and connectivities of grain boundaries play an important role in defining the main properties of materials across multiple scales. More recent mesoscale experiments and simulations provide large amounts of information about both geometric features and crystallography of the grain boundary network in material microstructures.

A classical model, due to Mullins and Herring,[26, 40, 41] for the evolution of grain boundaries in polycrystalline materials is based on the motion by mean curvature as the local evolution law. Mathematical analysis of the motion by mean curvature can be found, for instance in Refs. 11, 18, 19 and 23, and the study of the curvature flow for networks can be found in e.g. Refs. 14, 28, 29, 36, 37 and 38. In addition, to have a well-posed model of the evolution of the grain boundary network, one has to impose a separate condition at the triple junctions where three grain boundaries meet.[16, 29]

Grain growth is a very complex multiscale process. It involves, for example, dynamics of grain boundaries, triple junctions (triple junctions are where three grain boundaries meet) and the dynamics of lattice misorientations (difference in the orientation between two neighboring grains that share the grain boundary)/possibility of grains rotations. Recently, there are some studies that consider interactions among grain boundaries and triple junctions, e.g. Refs. 8, 44, 45, 49, 50 and 51. In our very recent work,[20, 21] we developed a new model for the evolution of the 2D grain-boundary network with finite mobility of the triple junctions and with dynamic lattice misorientations (possibility of grain rotations). In Refs. 20 and 21, using the energetic variational approach, we derived a system of geometric differential equations to describe the motion of such grain boundaries. Under assumption of no curvature effect, we established a local well-posedness result, as well as large time asymptotic behavior for the model. Our results included obtaining explicit energy decay rate for the system in terms of mobility of the triple junction and

the misorientation parameter (grains rotation relaxation time scale). In addition, we conducted several numerical experiments for the 2D grain boundary network in order to further understand/illustrate the effect of relaxation time scales of, for example, the curvature of grain boundaries, mobility of triple junctions, and dynamics of misorientations on how the grain boundary system decays energy and coarsens with time.[4, 20] In Ref. 4, we also presented and discussed relevant experimental results of grain growth in thin films. Note that in the work,[20, 21] the mathematical analysis of the model was done under assumption of no critical events/no disappearance events, e.g. grain disappearance, facet/grain boundary disappearance, facet interchange, splitting of unstable junctions (however, numerical simulations were performed with critical events).

The current work is motivated and is closely related to the work in Refs. 3, 5 and 6 where a reduced 1D coarsening model based on the dynamical system was studied for texture evolution and was used to identify texture evolution as a gradient flow, see also the article[31] for a perspective on the problem. In addition, this paper is a further extension of our work in Refs. 4, 20 and 21, and the work in Refs. 9, 10, 12, 30 and 46 is also relevant. In this paper, we study a stochastic model for the evolution of planar grain boundary network in order to be able to incorporate and model the effect of the critical events. Note, in general, an interaction among the grain boundaries and the triple junctions in a grain boundary network (including modeling of critical/disappearance events, e.g. grain disappearance, facet/grain boundary disappearance, facet interchange, splitting of unstable junctions) is a very complex process. However, in this work, we start with a simplified and more accessible for the mathematical analysis model and, hence, consider the Langevin equation analog of the model from Ref. 21, with the interactions among triple junctions and misorientations modeled as white noise. Next, we use the energetic variational approach to establish the associated fluctuation–dissipation theorem. The fluctuation–dissipation property ensures that the free energy of the corresponding Fokker–Planck system is dissipative. Moreover, the fluctuation–dissipation theorem also gives the sufficient condition for the steady-state solution of the Fokker–Planck equation to be given by the Boltzmann distribution.

Next, we study the well-posedness of the derived Fokker–Planck system under assumption of the fluctuation–dissipation relation. In particular, we show that the solution of the Fokker–Planck equation converges exponentially fast to the Boltzmann distribution for grain boundary energy of the system. Note that, the grain boundary energy has degeneracy with respect to the misorientations (due to constraints on misorientations) and singularity with respect to the triple junction. To overcome these difficulties, based on the idea of Ref. 39 (and see also a relevant work[24]), we consider Fokker–Planck equation in a weighted L^2 space, and we use the semigroup theory and the Poincaré inequality to obtain well-posedness and long-time asymptotics of the solution.

Finally, for an equilibrium configuration of a boundary network, we derive explicit local algebraic relations, a generalized Herring Condition formula, as well as formula that connects grain boundary energy density with the geometry of the grain boundaries that share a triple junction. The later local algebraic relation gives the condition for a steady-state solution of marginal probability density of misorientations to be the Boltzmann distribution with respect to a grain boundary energy density. Such a steady-state solution for marginal probability density of misorientations is related to the observed Boltzmann distribution for the steady-state Grain Boundary Character Distribution (GBCD) statistical metric of grain growth, e.g. Refs. 3, 5 and 6. Although the investigated simplified stochastic model neglects the explicit interactions and correlations among triple junctions, the considered specific form of the noise, under the fluctuation–dissipation assumption, provides partial information about evolution of a grain boundary network, and is consistent with extensive grain growth simulations presented in this paper.

The paper is organized as follows. In Sec. 2.1, we discuss important details and properties of the model for the grain boundary motion from Ref. 21. In Sec. 2.2, we introduce the stochastic model of the grain boundary system. In Sec. 3, we establish well-posedness results of the associated Fokker–Planck equation and obtain the long-time asymptotic behavior of the solution. In Sec. 4, we derive Fokker–Planck type equation for the marginal probability density of the misorientations and study long-time asymptotics of its solution. Finally, in Sec. 5, we present extensive numerical experiments to show consistency among the obtained results for the simplified stochastic model of a grain boundary network and the results of 2D grain growth simulations based on sharp-interface approach[20] (and an earlier work[3, 6]), including numerical investigation of the derived local algebraic relations for an equilibrium configuration of a boundary network.

2. The Fokker–Planck Equation and the Fluctuation–Dissipation Principle

In this section, we first derive a Langevin equation, a stochastic differential equation for the dynamics of misorientations and the triple junctions using the deterministic model of grain boundary motion obtained in Ref. 21 and see also Ref. 20. After that, we establish the fluctuation–dissipation theorem from associated Fokker–Planck equation. Note, we use below notation $|\cdot|$ for a standard Euclidean vector norm.

2.1. *Review of the deterministic model and the gradient flow structure*

First, we review here the deterministic grain boundary motion model from Ref. 21. Assume a single triple junction and consider the following grain boundary energy

of the system:

$$\tilde{E} = \sum_{j=1}^{3} \sigma(\Delta^{(j)}\alpha)|\Gamma_t^{(j)}|, \tag{2.1}$$

where $\sigma : \mathbb{R} \to \mathbb{R}$ is a given surface tension of a grain boundary, $\alpha^{(j)} = \alpha^{(j)}(t) : [0,\infty) \to \mathbb{R}$ is a time-dependent orientation of the grains, $\theta = \Delta^{(j)}\alpha := \alpha^{(j-1)} - \alpha^{(j)}$ is a lattice misorientation of the grain boundary $\Gamma_t^{(j)}$, and $|\Gamma_t^{(j)}|$ is the length of $\Gamma_t^{(j)}$ for $j = 1, 2, 3$. Here we put $\alpha^{(0)} = \alpha^{(3)}$. In this work, we assume a grain boundary energy density $\sigma(\Delta^{(j)}\alpha)$ is only a function of misorientation $\Delta^{(j)}\alpha$. In addition, we assume that σ is a C^1 function on $\mathbb{R}$.

Then, as a result of applying the maximal dissipation principle for the energy (2.1), the following model was derived in Ref. 21:

$$\begin{cases} v_n^{(j)} = \mu\sigma(\Delta^{(j)}\alpha)\kappa^{(j)}, \quad \text{on } \Gamma_t^{(j)},\ t > 0, \quad j = 1, 2, 3, \\ \dfrac{d\alpha^{(j)}}{dt} = -\gamma\Big(\sigma_\theta(\Delta^{(j+1)}\alpha)|\Gamma_t^{(j+1)}| - \sigma_\theta(\Delta^{(j)}\alpha)|\Gamma_t^{(j)}|\Big), \quad j = 1, 2, 3, \\ \dfrac{d\boldsymbol{a}}{dt}(t) = -\eta\displaystyle\sum_{k=1}^{3} \sigma(\Delta^{(k)}\alpha)\frac{\boldsymbol{b}^{(k)}}{|\boldsymbol{b}^{(k)}|}, \quad t > 0, \text{ at } \boldsymbol{a}, \\ \Gamma_t^{(j)} : \boldsymbol{\xi}^{(j)}(s,t), \quad 0 \le s \le 1, \quad t > 0, \quad j = 1, 2, 3, \\ \boldsymbol{a}(t) = \boldsymbol{\xi}^{(1)}(1,t) = \boldsymbol{\xi}^{(2)}(1,t) = \boldsymbol{\xi}^{(3)}(1,t), \quad \text{and} \quad \boldsymbol{\xi}^{(j)}(0,t) = \boldsymbol{x}^{(j)}, \quad j = 1, 2, 3, \end{cases} \tag{2.2}$$

where $\Delta^{(4)}\alpha = \Delta^{(1)}\alpha$. In (2.2), $v_n^{(j)}$, $\kappa^{(j)}$, and $\boldsymbol{b}^{(j)} = \boldsymbol{\xi}_s^{(j)}$ denote a normal velocity, a curvature and a tangent vector of the grain boundary $\Gamma_t^{(j)}$, respectively. Note that s is *not* an arc length parameter of $\Gamma_t^{(j)}$, namely, $\boldsymbol{b}^{(j)}$ is *not* necessarily a unit tangent vector. The vector $\boldsymbol{a} = \boldsymbol{a}(t) : [0,\infty) \to \mathbb{R}^2$ denotes a position of the triple junction, $\boldsymbol{x}^{(j)}$, in a current context (see also numerical Sec. 5), is a position of the end point of the grain boundary. The three independent relaxation time scales $\mu, \gamma, \eta > 0$ (length, misorientation and position of the triple junction) are considered in this work as positive constants.

Recall that in Ref. 21, to derive (2.2), we first computed energy dissipation rate,

$$\begin{aligned} \frac{d\tilde{E}}{dt} &= \frac{d}{dt}\sum_{j=1}^{3}\int_0^1 \sigma(\Delta^{(j)}\alpha(t))|\boldsymbol{b}^{(j)}(s,t)|\,ds \\ &= \sum_{j=1}^{3}\int_0^1 \sigma(\Delta^{(j)}\alpha(t))\frac{\boldsymbol{b}^{(j)}(s,t)}{|\boldsymbol{b}^{(j)}(s,t)|}\cdot\boldsymbol{\xi}_{ts}^{(j)}(s,t)\,ds \\ &\quad + \sum_{j=1}^{3}\int_0^1 \sigma_\theta(\Delta^{(j)}\alpha(t))(\Delta^{(j)}\alpha(t))_t|\boldsymbol{b}^{(j)}(s,t)|\,ds. \end{aligned} \tag{2.3}$$

Using $\boldsymbol{\xi}_{ts}^{(j)} = (\boldsymbol{\xi}_t^{(j)})_s$, integration by parts, $\boldsymbol{\xi}^{(j)}(0,t) = \boldsymbol{x}^{(j)}$ is independent of t, and $\boldsymbol{\xi}^{(j)}(1,t) = \boldsymbol{a}(t)$, we have

$$\begin{aligned}
&\sum_{j=1}^{3} \int_0^1 \sigma(\Delta^{(j)}\alpha(t)) \frac{\boldsymbol{b}^{(j)}(s,t)}{|\boldsymbol{b}^{(j)}(s,t)|} \cdot \boldsymbol{\xi}_{ts}^{(j)}(s,t)\, ds \\
&\quad = -\sum_{j=1}^{3} \sigma(\Delta^{(j)}\alpha(t)) \int_0^1 \left(\frac{\boldsymbol{b}^{(j)}(s,t)}{|\boldsymbol{b}^{(j)}(s,t)|} \right)_s \cdot \boldsymbol{\xi}_t^{(j)}(s,t)\, ds \\
&\qquad + \sum_{j=1}^{3} \sigma(\Delta^{(j)}\alpha(t)) \frac{\boldsymbol{b}^{(j)}(1,t)}{|\boldsymbol{b}^{(j)}(1,t)|} \cdot \boldsymbol{a}_t(t). \qquad (2.4)
\end{aligned}$$

Recall that $\Delta^{(j)}\alpha = \alpha^{(j-1)} - \alpha^{(j)}$, we replace index of sum for the misorientations and we obtain

$$\begin{aligned}
&\sum_{j=1}^{3} \int_0^1 \sigma_\theta(\Delta^{(j)}\alpha(t))(\Delta^{(j)}\alpha(t))_t |\boldsymbol{b}^{(j)}(s,t)|\, ds \\
&\quad = \sum_{j=1}^{3} \left(\sigma_\theta(\Delta^{(j+1)}\alpha(t))|\Gamma_t^{(j+1)}| - \sigma_\theta(\Delta^{(j)}\alpha(t))|\Gamma_t^{(j)}| \right) \alpha_t^{(j)}(t). \qquad (2.5)
\end{aligned}$$

Inserting (2.4) and (2.5) into (2.3), we have

$$\begin{aligned}
\frac{d\tilde{E}}{dt} &= -\sum_{j=1}^{3} \sigma(\Delta^{(j)}\alpha(t)) \int_0^1 \left(\frac{\boldsymbol{b}^{(j)}(s,t)}{|\boldsymbol{b}^{(j)}(s,t)|} \right)_s \cdot \boldsymbol{\xi}_t^{(j)}(s,t)\, ds \\
&\quad + \sum_{j=1}^{3} \sigma(\Delta^{(j)}\alpha(t)) \frac{\boldsymbol{b}^{(j)}(1,t)}{|\boldsymbol{b}^{(j)}(1,t)|} \cdot \boldsymbol{a}_t(t) \\
&\quad + \sum_{j=1}^{3} \left(\sigma_\theta(\Delta^{(j+1)}\alpha(t))|\Gamma_t^{(j+1)}| - \sigma_\theta(\Delta^{(j)}\alpha(t))|\Gamma_t^{(j)}| \right) \alpha_t^{(j)}(t). \qquad (2.6)
\end{aligned}$$

After that, we ensured that the entire system is dissipative, that is $\frac{d\tilde{E}}{dt} \leq 0$. We obtained (2.2) with a help of the Frenet–Serret formulas and with a help of the energy dissipation principle which took a form as presented below:

$$\frac{d\tilde{E}}{dt} = -\sum_{j=1}^{3} \left(\frac{1}{\mu} \int_{\Gamma_t^{(j)}} |v_n^{(j)}|^2 d\mathcal{H}^1 + \frac{1}{\gamma} \left| \frac{d\alpha^{(j)}}{dt}(t) \right|^2 \right) - \frac{1}{\eta} \left| \frac{d\boldsymbol{a}}{dt} \right|^2,$$

where $\mathcal{H}^1$ is the one-dimensional Hausdorff measure. More in-depth discussion and complete details of the derivation of the model (2.2) can be found in our earlier work (see Ref. 21, Sec. 2).

Next, in Ref. 21, we relaxed curvature effect, by taking the limit $\mu \to \infty$, and we obtained the reduced model:

$$\begin{cases} \dfrac{d\alpha^{(j)}}{dt} = -\gamma\Big(\sigma_\theta(\Delta^{(j+1)}\alpha)|\boldsymbol{a}(t) - \boldsymbol{x}^{(j+1)}| - \sigma_\theta(\Delta^{(j)}\alpha)|\boldsymbol{a}(t) - \boldsymbol{x}^{(j)}|\Big), \quad j = 1, 2, 3, \\ \dfrac{d\boldsymbol{a}}{dt}(t) = -\eta \displaystyle\sum_{j=1}^{3} \sigma(\Delta^{(j)}\alpha) \frac{\boldsymbol{a}(t) - \boldsymbol{x}^{(j)}}{|\boldsymbol{a}(t) - \boldsymbol{x}^{(j)}|}, \quad t > 0, \end{cases} \tag{2.7}$$

where $\boldsymbol{x}^{(4)} = \boldsymbol{x}^{(1)}$. Note, in Ref. 21, we first applied the maximal dissipation principle for the grain boundary energy of the system with curvature (2.1), and after that we took the relaxation limit $\mu \to \infty$. In fact, as the following proposition shows, these operations are interchangeable.

Proposition 2.1. *Let E be a relaxation energy associated with $\tilde{E}$ ($\mu \to \infty$), given by*

$$E(\Delta\boldsymbol{\alpha}, \boldsymbol{a}) = \sum_{j=1}^{3} \sigma(\Delta^{(j)}\alpha)|\boldsymbol{a} - \boldsymbol{x}^{(j)}|.$$

Then, equation (2.7) *is a gradient flow associated with the energy E, namely, we have,*

$$\begin{aligned} \frac{\delta E}{\delta \alpha^{(j)}} &= \sigma_\theta(\Delta^{(j+1)}\alpha)|\boldsymbol{a} - \boldsymbol{x}^{(j+1)}| - \sigma_\theta(\Delta^{(j)}\alpha)|\boldsymbol{a} - \boldsymbol{x}^{(j)}|, \\ \frac{\delta E}{\delta \boldsymbol{a}} &= \sum_{j=1}^{3} \sigma(\Delta^{(j)}\alpha) \frac{\boldsymbol{a} - \boldsymbol{x}^{(j)}}{|\boldsymbol{a} - \boldsymbol{x}^{(j)}|}. \end{aligned} \tag{2.8}$$

Proof. The first equation of (2.8) can be obtained by taking the derivative of E with respect to $\alpha^{(j)}$. The second equation of (2.8) can be deduced from,

$$\left.\frac{d}{d\varepsilon}\right|_{\varepsilon=0} E(\Delta\boldsymbol{\alpha}, \boldsymbol{a} + \varepsilon\boldsymbol{p}) = \sum_{j=1}^{3} \sigma(\Delta^{(j)}\alpha) \frac{\boldsymbol{a} - \boldsymbol{x}^{(j)}}{|\boldsymbol{a} - \boldsymbol{x}^{(j)}|} \cdot \boldsymbol{p},$$

for $\boldsymbol{p} \in \mathbb{R}^2$. □

To analyze the grain boundary motion in this work, Secs. 2.2–4, it will be convenient to use the misorientation $\Delta^{(j)}\alpha$ as a state variable, instead of the orientation $\alpha^{(j)}$. Thus, from the first equation of (2.7), we can derive

$$\begin{aligned} \frac{d(\Delta^{(j)}\alpha)}{dt} = -\gamma\Big(&2\sigma_\theta(\Delta^{(j)}\alpha)|\boldsymbol{a}(t) - \boldsymbol{x}^{(j)}| \\ &- \sigma_\theta(\Delta^{(j+1)}\alpha)|\boldsymbol{a}(t) - \boldsymbol{x}^{(j+1)}| - \sigma_\theta(\Delta^{(j-1)}\alpha)|\boldsymbol{a}(t) - \boldsymbol{x}^{(j-1)}|\Big), \end{aligned} \tag{2.9}$$

where $\Delta^{(0)}\alpha = \Delta^{(3)}\alpha$, $\Delta^{(1)}\alpha = \Delta^{(4)}\alpha$, $\Delta^{(2)}\alpha = \Delta^{(5)}\alpha$, and $\boldsymbol{x}^{(j)}$ is defined similarly. From the definition of the misorientation, $\Delta^{(j)}\alpha = \alpha^{(j-1)} - \alpha^{(j)}$, it is easy to find the constraint

$$\Delta^{(1)}\alpha + \Delta^{(2)}\alpha + \Delta^{(3)}\alpha = 0. \tag{2.10}$$

To consider (2.9) to be a gradient flow, we introduce the two-dimensional plane

$$\Omega := \left\{ \left(\Delta^{(1)}\alpha, \Delta^{(2)}\alpha, \Delta^{(3)}\alpha\right) \in \left(-\frac{\pi}{4}, \frac{\pi}{4}\right)^3 : \Delta^{(1)}\alpha + \Delta^{(2)}\alpha + \Delta^{(3)}\alpha = 0 \right\} \subset \mathbb{R}^3. \tag{2.11}$$

For planar grain boundary network, it is reasonable to consider such range of the misorientations. Note that the equation (2.7) is a system for the orientation and the triple junction. Now, using (2.9), we are going to show next that it also possesses the gradient flow structure of the misorientations.

Proposition 2.2. *The equation* (2.9) *has the gradient flow structure of the misorientation with the energy* E.

Proof. We need to show that the right-hand side of (2.9) is a gradient of E with respect to misorientation $\Delta\boldsymbol{\alpha}$ on Ω. Using the fact that one of the normal vectors of Ω is ${}^t(1,1,1)$, the tangential derivative for an arbitrary function $\phi = \phi(\Delta^{(1)}\alpha, \Delta^{(2)}\alpha, \Delta^{(3)}\alpha)$ on Ω is given by

$$\begin{aligned}\nabla^{\Omega}_{\Delta\boldsymbol{\alpha}}\phi &= \left(\begin{pmatrix} 1 & 0 & 0 \\ 0 & 1 & 0 \\ 0 & 0 & 1 \end{pmatrix} - \frac{1}{3}\begin{pmatrix} 1 & 1 & 1 \\ 1 & 1 & 1 \\ 1 & 1 & 1 \end{pmatrix}\right) \begin{pmatrix} \phi_{\Delta^{(1)}\alpha} \\ \phi_{\Delta^{(2)}\alpha} \\ \phi_{\Delta^{(3)}\alpha} \end{pmatrix} \\ &= \frac{1}{3}\begin{pmatrix} 2 & -1 & -1 \\ -1 & 2 & -1 \\ -1 & -1 & 2 \end{pmatrix} \begin{pmatrix} \phi_{\Delta^{(1)}\alpha} \\ \phi_{\Delta^{(2)}\alpha} \\ \phi_{\Delta^{(3)}\alpha} \end{pmatrix}. \end{aligned} \tag{2.12}$$

Thus, we have that

$$\nabla^{\Omega}_{\Delta\boldsymbol{\alpha}} E = \frac{1}{3}\begin{pmatrix} +2\sigma_\theta(\Delta^{(1)}\alpha)|\boldsymbol{a} - \boldsymbol{x}^{(1)}| - \sigma_\theta(\Delta^{(2)}\alpha)|\boldsymbol{a} - \boldsymbol{x}^{(2)}| - \sigma_\theta(\Delta^{(3)}\alpha)|\boldsymbol{a} - \boldsymbol{x}^{(3)}| \\ -\sigma_\theta(\Delta^{(1)}\alpha)|\boldsymbol{a} - \boldsymbol{x}^{(1)}| + 2\sigma_\theta(\Delta^{(2)}\alpha)|\boldsymbol{a} - \boldsymbol{x}^{(2)}| - \sigma_\theta(\Delta^{(3)}\alpha)|\boldsymbol{a} - \boldsymbol{x}^{(3)}| \\ -\sigma_\theta(\Delta^{(1)}\alpha)|\boldsymbol{a} - \boldsymbol{x}^{(1)}| - \sigma_\theta(\Delta^{(2)}\alpha)|\boldsymbol{a} - \boldsymbol{x}^{(2)}| + 2\sigma_\theta(\Delta^{(3)}\alpha)|\boldsymbol{a} - \boldsymbol{x}^{(3)}| \end{pmatrix}. \tag{2.13}$$

Hence, Eq. (2.9) can be regarded as a gradient flow of the energy E, that is

$$\frac{d}{dt}\begin{pmatrix} \Delta^{(1)}\alpha \\ \Delta^{(2)}\alpha \\ \Delta^{(3)}\alpha \end{pmatrix} = -3\gamma\nabla^{\Omega}_{\Delta\boldsymbol{\alpha}} E. \tag{2.14}$$

□

From Propositions 2.1 and 2.2, we have that

$$\frac{d(\Delta\boldsymbol{\alpha})}{dt} = -3\gamma\nabla^{\Omega}_{\Delta\boldsymbol{\alpha}}E, \quad \frac{d\boldsymbol{a}}{dt} = -\eta\nabla_{\boldsymbol{a}}E,$$

where $\Delta\boldsymbol{\alpha} = (\Delta^{(1)}\alpha, \Delta^{(2)}\alpha, \Delta^{(3)}\alpha)$. Thus, we obtain the following energy dissipation

$$\frac{dE}{dt} = -\frac{1}{3\gamma}\left|\frac{d(\Delta\boldsymbol{\alpha})}{dt}\right|^2 - \frac{1}{\eta}\left|\frac{d\boldsymbol{a}}{dt}\right|^2.$$

2.2. *Stochastic model and the fluctuation–dissipation theorem*

Here, we propose a simplified (and more accessible for the mathematical analysis) stochastic model to develop better understanding of dynamics of misorientations and triple junctions in a network. In our model, we consider ensemble of triple junctions and misorientations (without curvature effect), and we use white noise to describe interactions among them. Therefore, we consider the following Langevin equations, or stochastic differential equations,

$$\begin{aligned} d(\Delta\boldsymbol{\alpha}) &= \boldsymbol{v}_{\Delta\boldsymbol{\alpha}}\,dt + \beta_{\Delta\boldsymbol{\alpha}}\,dB, \quad \boldsymbol{v}_{\Delta\boldsymbol{\alpha}} = -3\gamma\nabla^{\Omega}_{\Delta\boldsymbol{\alpha}}E, \\ d\boldsymbol{a} &= \boldsymbol{v}_{\boldsymbol{a}}\,dt + \beta_{\boldsymbol{a}}\,dB, \quad \boldsymbol{v}_{\boldsymbol{a}} = -\eta\frac{\delta E}{\delta \boldsymbol{a}} = -\eta\nabla_{\boldsymbol{a}}E. \end{aligned} \tag{2.15}$$

Here B denotes a Brownian motion, and $\beta_{\Delta\boldsymbol{\alpha}}, \beta_{\boldsymbol{a}} > 0$ are fluctuation parameters for misorientation $\Delta\boldsymbol{\alpha}$ and triple junction $\boldsymbol{a}$, respectively. The proposed model (2.15) can be viewed as a stochastic analog of the "vertex model" (2.7). Thus, the associated probability density function or joint distribution function of misorientations $\Delta\boldsymbol{\alpha}$ and positions of the triple junctions $\boldsymbol{a}$, $f = f(\Delta\boldsymbol{\alpha}, \boldsymbol{a}, t)$ obeys the following Fokker–Planck equation,

$$\frac{\partial f}{\partial t} + \nabla^{\Omega}_{\Delta\boldsymbol{\alpha}}\cdot(\boldsymbol{v}_{\Delta\boldsymbol{\alpha}}f) + \nabla_{\boldsymbol{a}}\cdot(\boldsymbol{v}_{\boldsymbol{a}}f) = \frac{\beta^2_{\Delta\boldsymbol{\alpha}}}{2}\Delta^{\Omega}_{\Delta\boldsymbol{\alpha}}f + \frac{\beta^2_{\boldsymbol{a}}}{2}\Delta_{\boldsymbol{a}}f, \tag{2.16}$$

where $\Delta^{\Omega}_{\Delta\boldsymbol{\alpha}} = \nabla^{\Omega}_{\Delta\boldsymbol{\alpha}}\cdot\nabla^{\Omega}_{\Delta\boldsymbol{\alpha}}$, and $\Delta_{\boldsymbol{a}}$ is the standard Laplacian on Ω_{TJ}. Hereafter a bounded domain $\Omega_{\mathrm{TJ}} \subset \mathbb{R}^2$ denotes the state space for the triple junction $\boldsymbol{a}$. In addition, we impose the natural boundary conditions to preserve the total mass of f,

$$\begin{aligned} &f\nabla^{\Omega}_{\Delta\boldsymbol{\alpha}}\left(\log f + \frac{6\gamma}{\beta^2_{\Delta\boldsymbol{\alpha}}}E\right)\cdot\boldsymbol{\nu}_{\Delta\boldsymbol{\alpha}}\Big|_{\partial\Omega\times\Omega_{\mathrm{TJ}}} = 0, \\ &f\nabla_{\boldsymbol{a}}\left(\log f + \frac{2\eta}{\beta^2_{\boldsymbol{a}}}E\right)\cdot\boldsymbol{\nu}_{\boldsymbol{a}}\Big|_{\Omega\times\partial\Omega_{\mathrm{TJ}}} = 0, \end{aligned} \tag{2.17}$$

where $\boldsymbol{\nu}_{\Delta\boldsymbol{\alpha}}$ and $\boldsymbol{\nu}_{\boldsymbol{a}}$ are an outer unit normal vector to $\partial\Omega$ and $\partial\Omega_{\mathrm{TJ}}$, respectively. Next, we state a condition for the fluctuation parameters $\beta_{\Delta\boldsymbol{\alpha}}$ and $\beta_{\boldsymbol{a}}$ under which the system described by the Fokker–Planck equation (2.16) and (2.17) is dissipative.

Theorem 2.1. *Let f be a solution of the Fokker–Planck equation* (2.16) *and* (2.17) *with velocities $\boldsymbol{v}_{\Delta\boldsymbol{\alpha}}$, $\boldsymbol{v}_{\boldsymbol{a}}$ as defined in* (2.15)*. If in addition, the relaxation time scales and the fluctuation parameters satisfy the relation,*

$$\frac{6\gamma}{\beta^2_{\Delta\boldsymbol{\alpha}}} = \frac{2\eta}{\beta^2_{\boldsymbol{a}}}, \tag{2.18}$$

which in turn, determines the parameter D as

$$D := \frac{\beta^2_{\Delta\boldsymbol{\alpha}}}{6\gamma} = \frac{\beta^2_{\boldsymbol{a}}}{2\eta}, \tag{2.19}$$

then, the Fokker–Planck equation (2.16) *and* (2.17) *satisfies the following energy law*:

$$\begin{aligned}
&\frac{d}{dt}\iint_{\Omega\times\Omega_{\mathrm{TJ}}} (Df\log f + fE)\, d\Delta\boldsymbol{\alpha} d\boldsymbol{a} \\
&\quad = -\frac{\beta^2_{\Delta\boldsymbol{\alpha}}}{2D}\iint_{\Omega\times\Omega_{\mathrm{TJ}}} f\left|\nabla^{\Omega}_{\Delta\boldsymbol{\alpha}}\left(D\log f + E\right)\right|^2 d\Delta\boldsymbol{\alpha} d\boldsymbol{a} \\
&\qquad - \frac{\beta^2_{\boldsymbol{a}}}{2D}\iint_{\Omega\times\Omega_{\mathrm{TJ}}} f\left|\nabla_{\boldsymbol{a}}\left(D\log f + E\right)\right|^2 d\Delta\boldsymbol{\alpha} d\boldsymbol{a}.
\end{aligned} \tag{2.20}$$

Here, $\iint_{\Omega\times\Omega_{\mathrm{TJ}}}(Df\log f + fE)\, d\Delta\boldsymbol{\alpha} d\boldsymbol{a}$ represents the (scaled) free energy of the Fokker–Planck system (2.16) *and* (2.17)*.*

Proof. First, we use expression (2.15) for the velocities $\boldsymbol{v}_{\Delta\boldsymbol{\alpha}}$ and $\boldsymbol{v}_{\boldsymbol{a}}$ in the Fokker–Planck equation (2.16), and we have

$$\frac{\partial f}{\partial t} = \frac{\beta^2_{\Delta\boldsymbol{\alpha}}}{2}\nabla^{\Omega}_{\Delta\boldsymbol{\alpha}}\cdot\left(f\nabla^{\Omega}_{\Delta\boldsymbol{\alpha}}\left(\log f + \frac{6\gamma}{\beta^2_{\Delta\boldsymbol{\alpha}}}E\right)\right) + \frac{\beta^2_{\boldsymbol{a}}}{2}\nabla_{\boldsymbol{a}}\cdot\left(f\nabla_{\boldsymbol{a}}\left(\log f + \frac{2\eta}{\beta^2_{\boldsymbol{a}}}E\right)\right).$$

Next, we multiply the Fokker–Planck equation (2.16) by $D(1+\log f) + E$ and integrate over $\Omega\times\Omega_{\mathrm{TJ}}$. Note that

$$\frac{\partial f}{\partial t}\left(D(1+\log f) + E\right) = \frac{\partial}{\partial t}(Df\log f + fE). \tag{2.21}$$

Hence, using the natural boundary conditions (2.17), we have

$$\begin{aligned}
&\frac{d}{dt}\iint_{\Omega\times\Omega_{\mathrm{TJ}}} (Df\log f + fE)\, d\Delta\boldsymbol{\alpha} d\boldsymbol{a} \\
&\quad = -\frac{\beta^2_{\Delta\boldsymbol{\alpha}}}{2}\iint_{\Omega\times\Omega_{\mathrm{TJ}}}\left(f\nabla^{\Omega}_{\Delta\boldsymbol{\alpha}}\left(\log f + \frac{6\gamma}{\beta^2_{\Delta\boldsymbol{\alpha}}}E\right)\right) \\
&\qquad \cdot\nabla^{\Omega}_{\Delta\boldsymbol{\alpha}}\left(D\log f + E\right) d\Delta\boldsymbol{\alpha} d\boldsymbol{a} \\
&\qquad - \frac{\beta^2_{\boldsymbol{a}}}{2}\iint_{\Omega\times\Omega_{\mathrm{TJ}}}\left(f\nabla_{\boldsymbol{a}}\left(\log f + \frac{2\eta}{\beta^2_{\boldsymbol{a}}}E\right)\right)\cdot\nabla_{\boldsymbol{a}}\left(D\log f + E\right) d\Delta\boldsymbol{\alpha} d\boldsymbol{a}.
\end{aligned} \tag{2.22}$$

Finally, using (2.19), we have energy dissipation

$$\begin{aligned}
&\frac{d}{dt}\iint_{\Omega\times\Omega_{\mathrm{TJ}}} (Df\log f + fE)\, d\Delta\boldsymbol{\alpha} d\boldsymbol{a} \\
&\quad = -\frac{\beta_{\Delta\boldsymbol{\alpha}}^2}{2D}\iint_{\Omega\times\Omega_{\mathrm{TJ}}} f\left|\nabla_{\Delta\boldsymbol{\alpha}}^{\Omega}\left(D\log f + E\right)\right|^2 d\Delta\boldsymbol{\alpha} d\boldsymbol{a} \\
&\qquad - \frac{\beta_{\boldsymbol{a}}^2}{2D}\iint_{\Omega\times\Omega_{\mathrm{TJ}}} f\left|\nabla_{\boldsymbol{a}}\left(D\log f + E\right)\right|^2 d\Delta\boldsymbol{\alpha} d\boldsymbol{a}.
\end{aligned}$$

□

Remark 2.1. The condition (2.18) is related to the fluctuation–dissipation theorem.[17, 32] The system will approach the equilibrium state of the free energy $\iint_{\Omega\times\Omega_{\mathrm{TJ}}}(Df\log f + fE)\, d\Delta\boldsymbol{\alpha} d\boldsymbol{a}$ under the total mass constraint of f, which coincides with the Boltzmann distribution for the grain boundary energy E,

$$f_\infty(\Delta\boldsymbol{\alpha}, \boldsymbol{a}) = C_1 \exp\left(-\frac{E(\Delta\boldsymbol{\alpha}, \boldsymbol{a})}{D}\right), \tag{2.23}$$

for some constant $C_1 > 0$. Relation (2.18), which is also called the *fluctuation–dissipation principle*, ensures not only the dissipation structure (2.20), but also that the solution of the Fokker–Planck equation (2.16) and (2.17) converges to the Boltzmann distribution (2.23).

3. Well-Posedness of the Fokker–Planck Equation

In this section, we study well-posedness of the proposed Fokker–Planck model (2.16) under the fluctuation–dissipation relation (2.18), and the natural boundary conditions

$$\begin{cases}
\dfrac{\partial f}{\partial t} + \nabla_{\Delta\boldsymbol{\alpha}}^{\Omega}\cdot(\boldsymbol{v}_{\Delta\boldsymbol{\alpha}} f) + \nabla_{\boldsymbol{a}}\cdot(\boldsymbol{v}_{\boldsymbol{a}} f) = \dfrac{\beta_{\Delta\boldsymbol{\alpha}}^2}{2}\Delta_{\Delta\boldsymbol{\alpha}}^{\Omega} f + \dfrac{\beta_{\boldsymbol{a}}^2}{2}\Delta_{\boldsymbol{a}} f, \\
\qquad\qquad\qquad\qquad\qquad\qquad \Delta\boldsymbol{\alpha}\in\Omega,\ \boldsymbol{a}\in\Omega_{\mathrm{TJ}},\ t>0, \\
\boldsymbol{v}_{\Delta\boldsymbol{\alpha}} = -3\gamma\nabla_{\Delta\boldsymbol{\alpha}}^{\Omega} E, \\
\boldsymbol{v}_{\boldsymbol{a}} = -\eta\dfrac{\delta E}{\delta \boldsymbol{a}} = -\eta\nabla_{\boldsymbol{a}} E, \\
\left(\dfrac{\beta_{\Delta\boldsymbol{\alpha}}^2}{2}\nabla_{\Delta\boldsymbol{\alpha}}^{\Omega} f - \boldsymbol{v}_{\Delta\boldsymbol{\alpha}} f\right)\cdot\boldsymbol{\nu}_{\Delta\boldsymbol{\alpha}}\Big|_{\partial\Omega\times\Omega_{\mathrm{TJ}}} = 0, \\
\left(\dfrac{\beta_{\boldsymbol{a}}^2}{2}\nabla_{\boldsymbol{a}} f - \boldsymbol{v}_{\boldsymbol{a}} f\right)\cdot\boldsymbol{\nu}_{\boldsymbol{a}}\Big|_{\Omega\times\partial\Omega_{\mathrm{TJ}}} = 0, \\
f(\Delta\boldsymbol{\alpha}, \boldsymbol{a}, 0) = f_0(\Delta\boldsymbol{\alpha}, \boldsymbol{a}).
\end{cases} \tag{3.1}$$

Here, we assume that bounded domain $\Omega_{\mathrm{TJ}} \subset \mathbb{R}^2$ is a domain with C^2 boundary and that

$$\Omega := \Big\{ \Delta\boldsymbol{\alpha} = \Big(\Delta^{(1)}\alpha, \Delta^{(2)}\alpha, \Delta^{(3)}\alpha\Big) \in \Big(-\frac{\pi}{4}, \frac{\pi}{4}\Big)^3 : \Delta^{(1)}\alpha + \Delta^{(2)}\alpha + \Delta^{(3)}\alpha = 0 \Big\} \subset \mathbb{R}^3. \tag{3.2}$$

As in Sec. 2, the parameters $\beta_{\Delta\boldsymbol{\alpha}}$, $\beta_{\boldsymbol{a}}$, γ, and η are positive constants satisfying the fluctuation–dissipation relation (2.18). The vectors $\boldsymbol{\nu}_{\Delta\boldsymbol{\alpha}}$ and $\boldsymbol{\nu}_{\boldsymbol{a}}$ are an outer unit normal vector to $\partial\Omega$ and $\partial\Omega_{\mathrm{TJ}}$, respectively. Recall from Sec. 2 that the energy of the system E is given by

$$E(\Delta\boldsymbol{\alpha}, \boldsymbol{a}) = \sum_{j=1}^{3} \sigma(\Delta^{(j)}\alpha)|\boldsymbol{a} - \boldsymbol{x}^{(j)}|, \tag{3.3}$$

where grain boundary energy density σ is a given C^1 function and $\boldsymbol{x}^{(j)} \in \mathbb{R}^2$ is a fixed position for $j = 1, 2, 3$. The initial data $f_0 : \Omega \times \Omega_{\mathrm{TJ}} \to \mathbb{R}$ is assumed to be positive and

$$\int_{\Omega\times\Omega_{\mathrm{TJ}}} f_0(\Delta\boldsymbol{\alpha}, \boldsymbol{a})\, d\Delta\boldsymbol{\alpha} d\boldsymbol{a} = 1. \tag{3.4}$$

From the energy law (2.20), one can expect that the asymptotic profile $f_\infty = f_\infty(\Delta\boldsymbol{\alpha}, \boldsymbol{a})$ of (3.1) is given by

$$f_\infty(\Delta\boldsymbol{\alpha}, \boldsymbol{a}) = C_1 \exp\Big(-\frac{E(\Delta\boldsymbol{\alpha}, \boldsymbol{a})}{D}\Big), \tag{3.5}$$

for some constant $C_1 > 0$, where $D > 0$ is defined by (2.19). Since f is a probability density function, the constant C_1 satisfies

$$\frac{1}{C_1} = \iint_{\Omega\times\Omega_{\mathrm{TJ}}} \exp\Big(-\frac{E(\Delta\boldsymbol{\alpha}, \boldsymbol{a})}{D}\Big)\, d\Delta\boldsymbol{\alpha} d\boldsymbol{a}. \tag{3.6}$$

In order to show that solution of the Fokker–Planck equation (3.1) converges to f_∞, we will introduce the change of variable $g(\Delta\boldsymbol{\alpha}, \boldsymbol{a}, t)$,

$$f(\Delta\boldsymbol{\alpha}, \boldsymbol{a}, t) = g(\Delta\boldsymbol{\alpha}, \boldsymbol{a}, t) \exp\Big(-\frac{E(\Delta\boldsymbol{\alpha}, \boldsymbol{a})}{D}\Big), \tag{3.7}$$

and we will prove that g converges to the constant C_1.

It is important to note, that the grain boundary energy E may not belong to $H^2(\Omega \times \Omega_{\mathrm{TJ}})$, hence a solution of (3.1) will not be smooth in general. Thus, we will introduce the notion of a weak solution of (3.1), similar to (cf. Ref. 33).

Definition 3.1. A function $f : \Omega \times \Omega_{\mathrm{TJ}} \times [0,\infty) \to \mathbb{R}$ is a weak solution of (3.1) if,

$$f \in L^\infty(0,\infty; L^2(\Omega \times \Omega_{\mathrm{TJ}})) \quad \text{with } \nabla^{\Omega}_{\Delta\boldsymbol{\alpha}} f,\ \nabla_{\boldsymbol{a}} f \in L^2(0,\infty; L^2(\Omega \times \Omega_{\mathrm{TJ}})), \tag{3.8}$$

and

$$\begin{aligned}
&\iint_{\Omega\times\Omega_{\mathrm{TJ}}} f\phi\, d\Delta\boldsymbol{\alpha} d\boldsymbol{a}\Big|_{t=T} - \int_0^T dt \iint_{\Omega\times\Omega_{\mathrm{TJ}}} f\phi_t\, d\Delta\boldsymbol{\alpha} d\boldsymbol{a} \\
&\quad + \int_0^T dt \iint_{\Omega\times\Omega_{\mathrm{TJ}}} \left(\left(\frac{\beta^2_{\Delta\boldsymbol{\alpha}}}{2} \nabla^{\Omega}_{\Delta\boldsymbol{\alpha}} f - \boldsymbol{v}_{\Delta\boldsymbol{\alpha}} f \right) \cdot \nabla^{\Omega}_{\Delta\boldsymbol{\alpha}} \phi \right. \\
&\quad \left. + \left(\frac{\beta^2_{\boldsymbol{a}}}{2} \nabla_{\boldsymbol{a}} f - \boldsymbol{v}_{\boldsymbol{a}} f \right) \cdot \nabla_{\boldsymbol{a}} \phi \right) d\Delta\boldsymbol{\alpha} d\boldsymbol{a} \\
&\quad = \iint_{\Omega\times\Omega_{\mathrm{TJ}}} f_0\phi\, d\Delta\boldsymbol{\alpha} d\boldsymbol{a}\Big|_{t=0},
\end{aligned} \tag{3.9}$$

for all $\phi \in C^\infty(\overline{\Omega \times \Omega_{\mathrm{TJ}} \times [0,\infty)})$ and almost every $T > 0$.

We also recall Hölder's inequality (Ref. 25, p. 77) and Gronwall's inequality (Ref. 22, Appendix B) that we will use in our analysis below.

Lemma 3.1. (Hölder's inequality) *For functions $u \in L^p(\Omega \times \Omega_{\mathrm{TJ}})$, $v \in L^q(\Omega \times \Omega_{\mathrm{TJ}})$, $1/p + 1/q = 1$, we have that*

$$\iint_{\Omega\times\Omega_{\mathrm{TJ}}} uv\, d\Delta\boldsymbol{\alpha} d\boldsymbol{a} \le \left(\iint_{\Omega\times\Omega_{\mathrm{TJ}}} |u|^p\, d\Delta\boldsymbol{\alpha} d\boldsymbol{a} \right)^{1/p} \left(\iint_{\Omega\times\Omega_{\mathrm{TJ}}} |v|^q\, d\Delta\boldsymbol{\alpha} d\boldsymbol{a} \right)^{1/q}.$$

Lemma 3.2. (Gronwall's inequality) *Let $\zeta(\cdot)$ be a nonnegative, absolutely continuous function on $[0,T]$, which satisfies for a.e. t, the differential inequality*

$$\zeta'(t) \le \phi(t)\zeta(t),$$

where $\phi(t)$ are summable function on $[0,T]$. Then,

$$\zeta(t) \le e^{\int_0^t \phi(s)\, ds} \zeta(0),$$

for all $0 \le t \le T$.

3.1. *Uniqueness and existence of a weak solution to the Fokker–Planck equation*

Here, we establish uniqueness and existence of a weak solution to (3.1). First, uniqueness of a weak solution to (3.1) is considered. Since the Fokker–Planck

equation (3.1) is linear, it is enough to deduce that the solution is zero provided that the initial data is zero.

Proposition 3.1. *Let $f : \Omega \times \Omega_{\mathrm{TJ}} \times [0,\infty) \to \mathbb{R}$ be a weak solution of* (3.1) *with $f_0 = 0$. Assume that σ is a C^1 function on $\mathbb{R}$. Then $f = 0$ in $\Omega \times \Omega_{\mathrm{TJ}} \times [0,\infty)$.*

Proof. We give a formal proof. Take f as a test function for (3.1), namely, multiply (3.1) by f and integrate over $\Omega \times \Omega_{\mathrm{TJ}}$. Then, using integration by parts and the natural boundary conditions, we obtain that

$$\begin{aligned}
&\frac{1}{2}\frac{d}{dt}\iint_{\Omega\times\Omega_{\mathrm{TJ}}} |f|^2\, d\Delta\boldsymbol{\alpha} d\boldsymbol{a} \\
&\quad = -\frac{\beta^2_{\Delta\boldsymbol{\alpha}}}{2}\iint_{\Omega\times\Omega_{\mathrm{TJ}}} |\nabla^{\Omega}_{\Delta\boldsymbol{\alpha}} f|^2\, d\Delta\boldsymbol{\alpha} d\boldsymbol{a} - \frac{\beta^2_{\boldsymbol{a}}}{2}\iint_{\Omega\times\Omega_{\mathrm{TJ}}} |\nabla_{\boldsymbol{a}} f|^2\, d\Delta\boldsymbol{\alpha} d\boldsymbol{a} \\
&\qquad + \iint_{\Omega\times\Omega_{\mathrm{TJ}}} f\boldsymbol{v}_{\Delta\boldsymbol{\alpha}}\cdot\nabla^{\Omega}_{\Delta\boldsymbol{\alpha}} f d\Delta\boldsymbol{\alpha} d\boldsymbol{a} + \iint_{\Omega\times\Omega_{\mathrm{TJ}}} f\boldsymbol{v}_{\boldsymbol{a}}\cdot\nabla_{\boldsymbol{a}} f\, d\Delta\boldsymbol{\alpha} d\boldsymbol{a}. \qquad (3.10)
\end{aligned}$$

To estimate the third and the fourth terms on the right-hand side of (3.10), we use Young's inequality

$$\begin{aligned}
&\iint_{\Omega\times\Omega_{\mathrm{TJ}}} f\boldsymbol{v}_{\Delta\boldsymbol{\alpha}}\cdot\nabla^{\Omega}_{\Delta\boldsymbol{\alpha}} f\, d\Delta\boldsymbol{\alpha} d\boldsymbol{a} \\
&\quad \le \frac{\beta^2_{\Delta\boldsymbol{\alpha}}}{2}\iint_{\Omega\times\Omega_{\mathrm{TJ}}} |\nabla^{\Omega}_{\Delta\boldsymbol{\alpha}} f|^2\, d\Delta\boldsymbol{\alpha} d\boldsymbol{a} + \frac{1}{2\beta^2_{\Delta\boldsymbol{\alpha}}}\iint_{\Omega\times\Omega_{\mathrm{TJ}}} |f|^2|\boldsymbol{v}_{\Delta\boldsymbol{\alpha}}|^2\, d\Delta\boldsymbol{\alpha} d\boldsymbol{a} \\
&\quad \le \frac{\beta^2_{\Delta\boldsymbol{\alpha}}}{2}\iint_{\Omega\times\Omega_{\mathrm{TJ}}} |\nabla^{\Omega}_{\Delta\boldsymbol{\alpha}} f|^2\, d\Delta\boldsymbol{\alpha} d\boldsymbol{a} + \frac{\|\boldsymbol{v}_{\Delta\boldsymbol{\alpha}}\|^2_{\infty}}{2\beta^2_{\Delta\boldsymbol{\alpha}}}\iint_{\Omega\times\Omega_{\mathrm{TJ}}} |f|^2\, d\Delta\boldsymbol{\alpha} d\boldsymbol{a}, \qquad (3.11)
\end{aligned}$$

and similarly,

$$\begin{aligned}
\iint_{\Omega\times\Omega_{\mathrm{TJ}}} f\boldsymbol{v}_{\boldsymbol{a}}\cdot\nabla_{\boldsymbol{a}} f\, d\Delta\boldsymbol{\alpha} d\boldsymbol{a} &\le \frac{\beta^2_{\boldsymbol{a}}}{2}\iint_{\Omega\times\Omega_{\mathrm{TJ}}} |\nabla_{\boldsymbol{a}} f|^2\, d\Delta\boldsymbol{\alpha} d\boldsymbol{a} \\
&\quad + \frac{\|\boldsymbol{v}_{\boldsymbol{a}}\|^2_{\infty}}{2\beta^2_{\boldsymbol{a}}}\iint_{\Omega\times\Omega_{\mathrm{TJ}}} |f|^2\, d\Delta\boldsymbol{\alpha} d\boldsymbol{a}, \qquad (3.12)
\end{aligned}$$

where $\|\boldsymbol{v}_{\Delta\boldsymbol{\alpha}}\|_{\infty} = \sup_{\Omega\times\Omega_{\mathrm{TJ}}} |\boldsymbol{v}_{\Delta\boldsymbol{\alpha}}|$ and $\|\boldsymbol{v}_{\boldsymbol{a}}\|_{\infty} = \sup_{\Omega\times\Omega_{\mathrm{TJ}}} |\boldsymbol{v}_{\boldsymbol{a}}|$. Thus, we have that

$$\frac{d}{dt}\iint_{\Omega\times\Omega_{\mathrm{TJ}}} |f|^2\, d\Delta\boldsymbol{\alpha} d\boldsymbol{a} \le \left(\frac{\|\boldsymbol{v}_{\Delta\boldsymbol{\alpha}}\|^2_{\infty}}{\beta^2_{\Delta\boldsymbol{\alpha}}} + \frac{\|\boldsymbol{v}_{\boldsymbol{a}}\|^2_{\infty}}{\beta^2_{\boldsymbol{a}}}\right)\iint_{\Omega\times\Omega_{\mathrm{TJ}}} |f|^2\, d\Delta\boldsymbol{\alpha} d\boldsymbol{a}. \qquad (3.13)$$

Therefore, the assertion of the proposition follows from the application of Gronwall's inequality. □

Next, we show existence of a weak solution to the Fokker–Planck equation (3.1). To do that, we use change of variable (3.7) and we derive the equation of g. By direct calculation of the derivative of f and the fluctuation–dissipation relation (2.18) and (2.19), we obtain

$$\begin{aligned}
\frac{\partial f}{\partial t} &= \frac{\partial g}{\partial t}\exp\left(-\frac{E}{D}\right),\\
\nabla^{\Omega}_{\Delta\boldsymbol{\alpha}}\cdot(\boldsymbol{v}_{\Delta\boldsymbol{\alpha}}f) &= \left(g(\nabla^{\Omega}_{\Delta\boldsymbol{\alpha}}\cdot\boldsymbol{v}_{\Delta\boldsymbol{\alpha}}) + \boldsymbol{v}_{\Delta\boldsymbol{\alpha}}\cdot\nabla^{\Omega}_{\Delta\boldsymbol{\alpha}}g - \frac{g}{D}\boldsymbol{v}_{\Delta\boldsymbol{\alpha}}\cdot\nabla^{\Omega}_{\Delta\boldsymbol{\alpha}}E\right)\exp\left(-\frac{E}{D}\right)\\
&= \left(-3\gamma g\Delta^{\Omega}_{\Delta\boldsymbol{\alpha}}E - 3\gamma\nabla^{\Omega}_{\Delta\boldsymbol{\alpha}}E\cdot\nabla^{\Omega}_{\Delta\boldsymbol{\alpha}}g + \frac{3\gamma g}{D}|\nabla^{\Omega}_{\Delta\boldsymbol{\alpha}}E|^2\right)\exp\left(-\frac{E}{D}\right),\\
\frac{\beta^2_{\Delta\boldsymbol{\alpha}}}{2}\Delta^{\Omega}_{\Delta\boldsymbol{\alpha}}f &= \frac{\beta^2_{\Delta\boldsymbol{\alpha}}}{2}\left(\Delta^{\Omega}_{\Delta\boldsymbol{\alpha}}g - \frac{2}{D}\nabla^{\Omega}_{\Delta\boldsymbol{\alpha}}E\cdot\nabla^{\Omega}_{\Delta\boldsymbol{\alpha}}g - \frac{g}{D}\Delta^{\Omega}_{\Delta\boldsymbol{\alpha}}E + \frac{g}{D^2}|\nabla^{\Omega}_{\Delta\boldsymbol{\alpha}}E|^2\right)\\
&\quad\times\exp\left(-\frac{E}{D}\right)\\
&= \left(3\gamma D\Delta^{\Omega}_{\Delta\boldsymbol{\alpha}}g - 6\gamma\nabla^{\Omega}_{\Delta\boldsymbol{\alpha}}E\cdot\nabla^{\Omega}_{\Delta\boldsymbol{\alpha}}g - 3\gamma g\Delta^{\Omega}_{\Delta\boldsymbol{\alpha}}E + \frac{3\gamma g}{D}|\nabla^{\Omega}_{\Delta\boldsymbol{\alpha}}E|^2\right)\\
&\quad\times\exp\left(-\frac{E}{D}\right),
\end{aligned}\tag{3.14}$$

Similarly, we have that

$$\begin{aligned}
\nabla_{\boldsymbol{a}}\cdot(\boldsymbol{v}_{\boldsymbol{a}}f) &= \left(-\eta g\Delta_{\boldsymbol{a}}E - \eta\nabla_{\boldsymbol{a}}E\cdot\nabla_{\boldsymbol{a}}g + \frac{\eta g}{D}|\nabla_{\boldsymbol{a}}E|^2\right)\exp\left(-\frac{E}{D}\right),\\
\frac{\beta^2_{\boldsymbol{a}}}{2}\Delta_{\boldsymbol{a}}f &= \left(\eta D\Delta_{\boldsymbol{a}}g - 2\eta\nabla_{\boldsymbol{a}}E\cdot\nabla_{\boldsymbol{a}}g - \eta g\Delta_{\boldsymbol{a}}E + \frac{\eta g}{D}|\nabla_{\boldsymbol{a}}E|^2\right)\exp\left(-\frac{E}{D}\right).
\end{aligned}\tag{3.15}$$

Thus, using (3.7), (3.14) and (3.15) in the Fokker–Planck equation (3.1), we arrive at the equation for the function g,

$$\frac{\partial g}{\partial t} = 3\gamma D\Delta^{\Omega}_{\Delta\boldsymbol{\alpha}}g + \eta D\Delta_{\boldsymbol{a}}g - 3\gamma\nabla^{\Omega}_{\Delta\boldsymbol{\alpha}}E\cdot\nabla^{\Omega}_{\Delta\boldsymbol{\alpha}}g - \eta\nabla_{\boldsymbol{a}}E\cdot\nabla_{\boldsymbol{a}}g.\tag{3.16}$$

We also derive the boundary condition for g using expression for the boundary conditions (3.1) for f. By direct computation and the fluctuation–dissipation relation (2.18) and (2.19), we have that

$$\begin{aligned}
\frac{\beta^2_{\Delta\boldsymbol{\alpha}}}{2}\nabla^{\Omega}_{\Delta\boldsymbol{\alpha}}f - \boldsymbol{v}_{\Delta\boldsymbol{\alpha}}f &= \left(\frac{\beta^2_{\Delta\boldsymbol{\alpha}}}{2}\nabla^{\Omega}_{\Delta\boldsymbol{\alpha}}g - \frac{\beta^2_{\Delta\boldsymbol{\alpha}}}{2D}g\nabla^{\Omega}_{\Delta\boldsymbol{\alpha}}E + 3\gamma g\nabla^{\Omega}_{\Delta\boldsymbol{\alpha}}E\right)\exp\left(-\frac{E}{D}\right)\\
&= 3\gamma D\exp\left(-\frac{E}{D}\right)\nabla^{\Omega}_{\Delta\boldsymbol{\alpha}}g,
\end{aligned}$$

$$\begin{aligned}\frac{\beta_{\boldsymbol{a}}^2}{2}\nabla_{\boldsymbol{a}} f - \boldsymbol{v}_{\boldsymbol{a}} f &= \left(\frac{\beta_{\boldsymbol{a}}^2}{2}\nabla_{\boldsymbol{a}} g - \frac{\beta_{\boldsymbol{a}}^2}{2D} g\nabla_{\boldsymbol{a}} E + \eta g \nabla_{\boldsymbol{a}} E\right)\exp\left(-\frac{E}{D}\right)\\ &= \eta D \exp\left(-\frac{E}{D}\right)\nabla_{\boldsymbol{a}} g.\end{aligned} \tag{3.17}$$

Thus, the natural boundary conditions for f is transformed into the Neumann boundary conditions for g. To study (3.16), we introduce a differential operator

$$Lg := 3\gamma D\Delta_{\Delta\boldsymbol{\alpha}}^{\Omega} g + \eta D\Delta_{\boldsymbol{a}} g - 3\gamma\nabla_{\Delta\boldsymbol{\alpha}}^{\Omega} E\cdot\nabla_{\Delta\boldsymbol{\alpha}}^{\Omega} g - \eta\nabla_{\boldsymbol{a}} E\cdot\nabla_{\boldsymbol{a}} g \tag{3.18}$$

subject to the Neumann boundary conditions

$$\begin{aligned}&\nabla_{\Delta\boldsymbol{\alpha}}^{\Omega} g\cdot\boldsymbol{\nu}_{\Delta\boldsymbol{\alpha}} = 0, \quad \text{on } \partial\Omega\times\Omega_{\mathrm{TJ}},\\ &\nabla_{\boldsymbol{a}} g\cdot\boldsymbol{\nu}_{\boldsymbol{a}} = 0, \qquad \text{on } \Omega\times\partial\Omega_{\mathrm{TJ}}.\end{aligned} \tag{3.19}$$

We will use the Lax–Milgram theorem below to show that L is a self-adjoint operator (cf. Ref. 25, Theorem 5.8). For the reader's convenience, we will state theorem below.

Lemma 3.3. (Lax–Milgram) *Let* $\mathbf{B}$ *be a bounded, coercive bilinear form on a Hilbert space* H*. Then for every bounded linear functional* $F\in H^*$*, there exists a unique element* $f\in H$ *such that* $\mathbf{B}(x,f) = F(x)$ *for all* $x\in H$*.*

Now, we proceed to show that L is a self-adjoint operator on the weighted L^2 spaces,

$$L^2(\Omega\times\Omega_{\mathrm{TJ}},\, dm), \quad dm = e^{-\frac{E}{D}}\, d\Delta\boldsymbol{\alpha} d\boldsymbol{a}. \tag{3.20}$$

Proposition 3.2. *Let* $dm = e^{-\frac{E}{D}}\, d\Delta\boldsymbol{\alpha} d\boldsymbol{a}$ *and let* L *be defined by* (3.18) *on* $L^2(\Omega\times\Omega_{\mathrm{TJ}}, dm)$ *with a domain* $D(L) := H^2(\Omega\times\Omega_{\mathrm{TJ}}, dm)$*, and with the Neumann boundary conditions* (3.19)*. Then,* L *is a self-adjoint operator on* $L^2(\Omega\times\Omega_{\mathrm{TJ}}, dm)$*.*

Proof. For $g_1,\, g_2\in D(L)$, we have by the definition of L, that,

$$\begin{aligned}&(Lg_1, g_2)_{L^2(\Omega\times\Omega_{\mathrm{TJ}}, dm)}\\ &\quad= 3\gamma D\iint_{\Omega\times\Omega_{\mathrm{TJ}}}\Delta_{\Delta\boldsymbol{\alpha}}^{\Omega} g_1 g_2\exp\left(-\frac{E}{D}\right) d\Delta\boldsymbol{\alpha} d\boldsymbol{a}\\ &\qquad+\eta D\iint_{\Omega\times\Omega_{\mathrm{TJ}}}\Delta_{\boldsymbol{a}} g_1 g_2\exp\left(-\frac{E}{D}\right) d\Delta\boldsymbol{\alpha} d\boldsymbol{a}\\ &\qquad- 3\gamma\iint_{\Omega\times\Omega_{\mathrm{TJ}}}\nabla_{\Delta\boldsymbol{\alpha}}^{\Omega} E\cdot\nabla_{\Delta\boldsymbol{\alpha}}^{\Omega} g_1 g_2\exp\left(-\frac{E}{D}\right) d\Delta\boldsymbol{\alpha} d\boldsymbol{a}\\ &\qquad-\eta\iint_{\Omega\times\Omega_{\mathrm{TJ}}}\nabla_{\boldsymbol{a}} E\cdot\nabla_{\boldsymbol{a}} g_1 g_2\exp\left(-\frac{E}{D}\right) d\Delta\boldsymbol{\alpha} d\boldsymbol{a}.\end{aligned} \tag{3.21}$$

Using the integration by parts for the first and the second terms on the right-hand side of (3.21), we obtain

$$\begin{aligned}
&\iint_{\Omega\times\Omega_{\mathrm{TJ}}} \Delta^{\Omega}_{\Delta\boldsymbol{\alpha}} g_1 g_2 \exp\left(-\frac{E}{D}\right) d\Delta\boldsymbol{\alpha} d\boldsymbol{a} \\
&\quad = -\iint_{\Omega\times\Omega_{\mathrm{TJ}}} \nabla^{\Omega}_{\Delta\boldsymbol{\alpha}} g_1 \cdot \nabla^{\Omega}_{\Delta\boldsymbol{\alpha}} \left(g_2 \exp\left(-\frac{E}{D}\right)\right) d\Delta\boldsymbol{\alpha} d\boldsymbol{a}, \quad \text{and} \\
&\iint_{\Omega\times\Omega_{\mathrm{TJ}}} \Delta_{\boldsymbol{a}} g_1 g_2 \exp\left(-\frac{E}{D}\right) d\Delta\boldsymbol{\alpha} d\boldsymbol{a} \\
&\quad = -\iint_{\Omega\times\Omega_{\mathrm{TJ}}} \nabla_{\boldsymbol{a}} g_1 \cdot \nabla_{\boldsymbol{a}} \left(g_2 \exp\left(-\frac{E}{D}\right)\right) d\Delta\boldsymbol{\alpha} d\boldsymbol{a}.
\end{aligned} \tag{3.22}$$

Since,

$$\begin{aligned}
\nabla^{\Omega}_{\Delta\boldsymbol{\alpha}} \left(g_2 \exp\left(-\frac{E}{D}\right)\right) &= \exp\left(-\frac{E}{D}\right) \nabla^{\Omega}_{\Delta\boldsymbol{\alpha}} g_2 - \frac{g_2}{D} \exp\left(-\frac{E}{D}\right) \nabla^{\Omega}_{\Delta\boldsymbol{\alpha}} E, \quad \text{and} \\
\nabla_{\boldsymbol{a}} \left(g_2 \exp\left(-\frac{E}{D}\right)\right) &= \exp\left(-\frac{E}{D}\right) \nabla_{\boldsymbol{a}} g_2 - \frac{g_2}{D} \exp\left(-\frac{E}{D}\right) \nabla_{\boldsymbol{a}} E,
\end{aligned}$$

the integrals of $\nabla^{\Omega}_{\Delta\boldsymbol{\alpha}} E \cdot \nabla^{\Omega}_{\Delta\boldsymbol{\alpha}} g_1 g_2 \exp(-\frac{E}{D})$ and $\nabla_{\boldsymbol{a}} E \cdot \nabla_{\boldsymbol{a}} g_1 g_2 \exp(-\frac{E}{D})$ cancel out. Thus, by the definition of dm,

$$\begin{aligned}
&(Lg_1, g_2)_{L^2(\Omega\times\Omega_{\mathrm{TJ}}, dm)} \\
&\quad = -3\gamma D \iint_{\Omega\times\Omega_{\mathrm{TJ}}} \nabla^{\Omega}_{\Delta\boldsymbol{\alpha}} g_1 \cdot \nabla^{\Omega}_{\Delta\boldsymbol{\alpha}} g_2 \exp\left(-\frac{E}{D}\right) d\Delta\boldsymbol{\alpha} d\boldsymbol{a} \\
&\qquad - \eta D \iint_{\Omega\times\Omega_{\mathrm{TJ}}} \nabla_{\boldsymbol{a}} g_1 \cdot \nabla_{\boldsymbol{a}} g_2 \exp\left(-\frac{E}{D}\right) d\Delta\boldsymbol{\alpha} d\boldsymbol{a} \\
&\quad = -3\gamma D \iint_{\Omega\times\Omega_{\mathrm{TJ}}} \nabla^{\Omega}_{\Delta\boldsymbol{\alpha}} g_1 \cdot \nabla^{\Omega}_{\Delta\boldsymbol{\alpha}} g_2 \, dm - \eta D \iint_{\Omega\times\Omega_{\mathrm{TJ}}} \nabla_{\boldsymbol{a}} g_1 \cdot \nabla_{\boldsymbol{a}} g_2 \, dm,
\end{aligned} \tag{3.23}$$

hence L is a dissipative symmetric operator.

Next, we show that L is maximal operator: for fixed $F \in L^2(\Omega \times \Omega_{\mathrm{TJ}}, dm)$, we show that there is $g \in H^2(\Omega \times \Omega_{\mathrm{TJ}}, dm)$, such that $-Lg + g = F$. Let us define for $g, \varphi \in H^1(\Omega \times \Omega_{\mathrm{TJ}}, dm)$,

$$\begin{aligned}
\langle -Lg + g, \varphi \rangle := 3\gamma D \iint_{\Omega\times\Omega_{\mathrm{TJ}}} &\nabla^{\Omega}_{\Delta\boldsymbol{\alpha}} g \cdot \nabla^{\Omega}_{\Delta\boldsymbol{\alpha}} \varphi \, dm \\
&+ \eta D \iint_{\Omega\times\Omega_{\mathrm{TJ}}} \nabla_{\boldsymbol{a}} g \cdot \nabla_{\boldsymbol{a}} \varphi \, dm + \iint_{\Omega\times\Omega_{\mathrm{TJ}}} g\varphi \, dm.
\end{aligned}$$

By Hölder's inequality and the definition of the Sobolev spaces, there is a positive constant $C_2 > 0$, such that for, $g, \varphi \in H^1(\Omega \times \Omega_{\mathrm{TJ}}, dm)$, we have that

$$\begin{aligned}|\langle -Lg + g, \varphi\rangle| &\leq 3\gamma D \|\nabla^{\Omega}_{\Delta\boldsymbol{\alpha}} g\|_{L^2(\Omega\times\Omega_{\mathrm{TJ}},dm)} \|\nabla^{\Omega}_{\Delta\boldsymbol{\alpha}} \varphi\|_{L^2(\Omega\times\Omega_{\mathrm{TJ}},dm)} \\ &\quad + \eta D \|\nabla_{\boldsymbol{a}} g\|_{L^2(\Omega\times\Omega_{\mathrm{TJ}},dm)} \|\nabla_{\boldsymbol{a}} \varphi\|_{L^2(\Omega\times\Omega_{\mathrm{TJ}},dm)} \\ &\quad + \|g\|_{L^2(\Omega\times\Omega_{\mathrm{TJ}},dm)} \|\varphi\|_{L^2(\Omega\times\Omega_{\mathrm{TJ}},dm)} \\ &\leq C_2 \|g\|_{H^1(\Omega\times\Omega_{\mathrm{TJ}},dm)} \|\varphi\|_{H^1(\Omega\times\Omega_{\mathrm{TJ}},dm)}.\end{aligned}$$

Thus, $\langle -Lg + g, \varphi\rangle$ is a bounded bilinear form in $H^1(\Omega \times \Omega_{\mathrm{TJ}}, dm)$. Also, for $g \in H^1(\Omega \times \Omega_{\mathrm{TJ}}, dm)$, we can obtain

$$\begin{aligned}\langle -Lg + g, g\rangle &= 3\gamma D \|\nabla^{\Omega}_{\Delta\boldsymbol{\alpha}} g\|^2_{L^2(\Omega\times\Omega_{\mathrm{TJ}},dm)} + \eta D \|\nabla_{\boldsymbol{a}} g\|^2_{L^2(\Omega\times\Omega_{\mathrm{TJ}},dm)} \\ &\quad + \|g\|^2_{L^2(\Omega\times\Omega_{\mathrm{TJ}},dm)} \\ &\geq \min\{3\gamma D, \eta D, 1\} \|g\|^2_{H^1(\Omega\times\Omega_{\mathrm{TJ}},dm)},\end{aligned}$$

which shows that $\langle -Lg + g, \varphi\rangle$ is a coercive bilinear form. In addition, the inner product $(F, \varphi)_{L^2(\Omega\times\Omega_{\mathrm{TJ}},dm)} : L^2(\Omega \times \Omega_{\mathrm{TJ}}, dm) \to \mathbb{R}$ can be regarded as a bounded linear functional in $H^1(\Omega \times \Omega_{\mathrm{TJ}}, dm)$, because for $\varphi \in H^1(\Omega \times \Omega_{\mathrm{TJ}}, dm)$, we have,

$$\begin{aligned}|(F, \varphi)_{L^2(\Omega\times\Omega_{\mathrm{TJ}},dm)}| &\leq \|F\|_{L^2(\Omega\times\Omega_{\mathrm{TJ}},dm)} \|\varphi\|_{L^2(\Omega\times\Omega_{\mathrm{TJ}},dm)} \\ &\leq \|F\|_{L^2(\Omega\times\Omega_{\mathrm{TJ}},dm)} \|\varphi\|_{H^1(\Omega\times\Omega_{\mathrm{TJ}},dm)}\end{aligned}$$

by Hölder's inequality. Thus, by the Lax–Milgram theorem, there exists $g \in H^1(\Omega \times \Omega_{\mathrm{TJ}}, dm)$ such that

$$\langle -Lg + g, \varphi\rangle = (F, \varphi)_{L^2(\Omega\times\Omega_{\mathrm{TJ}},\, dm)}$$

for $\varphi \in H^1(\Omega \times \Omega_{\mathrm{TJ}}, dm)$. Next, for arbitrary $\phi \in H^1(\Omega \times \Omega_{\mathrm{TJ}})$, take $\varphi = \phi \exp(\frac{E}{D}) \in H^1(\Omega \times \Omega_{\mathrm{TJ}}, dm)$. Then, we find that g is a weak solution of $-Lg + g = F$ with the Neumann boundary condition $\nabla^{\Omega}_{\Delta\boldsymbol{\alpha}} g \cdot \boldsymbol{\nu}_{\Delta\boldsymbol{\alpha}}|_{\partial\Omega\times\Omega_{\mathrm{TJ}}} = 0$, and $\nabla_{\boldsymbol{a}} g \cdot \boldsymbol{\nu}_{\boldsymbol{a}}|_{\Omega\times\partial\Omega_{\mathrm{TJ}}} = 0$. In a similar manner as for Ref. 25, we have $g \in H^2(\Omega \times \Omega_{\mathrm{TJ}})$. Since $\exp(-\frac{E}{D})$ is bounded, g belongs to $H^2(\Omega \times \Omega_{\mathrm{TJ}}, dm)$. □

By the semigroup theory (cf. Ref. 15), for any $g_0 \in L^2(\Omega \times \Omega_{\mathrm{TJ}}, dm)$, there uniquely exists $g \in C([0, \infty); L^2(\Omega \times \Omega_{\mathrm{TJ}}, dm)) \cap C^1((0, \infty); L^2(\Omega \times \Omega_{\mathrm{TJ}}, dm)) \cap C((0, \infty); H^2(\Omega \times \Omega_{\mathrm{TJ}}, dm))$ such that

$$\begin{cases} g_t = Lg, \quad t > 0, \\ g(0) = g_0. \end{cases} \tag{3.24}$$

Furthermore g belongs to $C^k((0, \infty); D(L^l))$ for any positive integer k, l. Using the existence of a solution of (3.24), one can obtain existence of a weak solution of (3.1).

Proposition 3.3. *Let $f_0 \in L^2(\Omega \times \Omega_{\mathrm{TJ}})$. Assume that σ is a C^1 function on $\mathbb{R}$. Then, there exists a weak solution f of* (3.1).

Proof. Let $g_0 = f_0 \exp(\frac{E}{D})$. Then $g_0 \in L^2(\Omega \times \Omega_{\mathrm{TJ}}, dm)$ hence there is a solution $g \in C([0,\infty); L^2(\Omega \times \Omega_{\mathrm{TJ}}, dm)) \cap C^1((0,\infty); L^2(\Omega \times \Omega_{\mathrm{TJ}}, dm)) \cap C((0,\infty); H^2(\Omega \times \Omega_{\mathrm{TJ}}, dm))$ to (3.24). Then by (3.23), for any $\phi \in C^\infty(\overline{\Omega \times \Omega_{\mathrm{TJ}} \times [0,\infty)})$ and almost every $T > 0$, we have that

$$\begin{aligned}
&\iint_{\Omega\times\Omega_{\mathrm{TJ}}} g\phi \exp\left(-\frac{E}{D}\right) d\Delta\boldsymbol{\alpha} d\boldsymbol{a}\Big|_{t=T} - \int_0^T dt \iint_{\Omega\times\Omega_{\mathrm{TJ}}} g\phi_t \exp\left(-\frac{E}{D}\right) d\Delta\boldsymbol{\alpha} d\boldsymbol{a} \\
&\quad + \int_0^T dt \iint_{\Omega\times\Omega_{\mathrm{TJ}}} \left(3\gamma D \nabla^{\Omega}_{\Delta\boldsymbol{\alpha}} g \cdot \nabla^{\Omega}_{\Delta\boldsymbol{\alpha}} \phi + \eta D \nabla_{\boldsymbol{a}} g \cdot \nabla_{\boldsymbol{a}} \phi\right) \exp\left(-\frac{E}{D}\right) d\Delta\boldsymbol{\alpha} d\boldsymbol{a} \\
&= \iint_{\Omega\times\Omega_{\mathrm{TJ}}} g_0\phi \exp\left(-\frac{E}{D}\right) d\Delta\boldsymbol{\alpha} d\boldsymbol{a}\Big|_{t=0}. \qquad (3.25)
\end{aligned}$$

From (3.21), (3.22), and (3.23) with $g_1 = \phi$, $g_2 = g$, we deduce

$$\begin{aligned}
&\iint_{\Omega\times\Omega_{\mathrm{TJ}}} \left(3\gamma D \nabla^{\Omega}_{\Delta\boldsymbol{\alpha}} g \cdot \nabla^{\Omega}_{\Delta\boldsymbol{\alpha}} \phi + \eta D \nabla_{\boldsymbol{a}} g \cdot \nabla_{\boldsymbol{a}} \phi\right) \exp\left(-\frac{E}{D}\right) d\Delta\boldsymbol{\alpha} d\boldsymbol{a} \\
&\quad = -(L\phi, g)_{L^2(\Omega\times\Omega_{\mathrm{TJ}}, dm)} \\
&\quad = 3\gamma D \iint_{\Omega\times\Omega_{\mathrm{TJ}}} \nabla^{\Omega}_{\Delta\boldsymbol{\alpha}} \phi \cdot \nabla^{\Omega}_{\Delta\boldsymbol{\alpha}} \left(g \exp\left(-\frac{E}{D}\right)\right) d\Delta\boldsymbol{\alpha} d\boldsymbol{a} \\
&\qquad + \eta D \iint_{\Omega\times\Omega_{\mathrm{TJ}}} \nabla_{\boldsymbol{a}} \phi \cdot \nabla_{\boldsymbol{a}} \left(g \exp\left(-\frac{E}{D}\right)\right) d\Delta\boldsymbol{\alpha} d\boldsymbol{a} \\
&\qquad + 3\gamma \iint_{\Omega\times\Omega_{\mathrm{TJ}}} \nabla^{\Omega}_{\Delta\boldsymbol{\alpha}} E \cdot \nabla^{\Omega}_{\Delta\boldsymbol{\alpha}} \phi g \exp\left(-\frac{E}{D}\right) d\Delta\boldsymbol{\alpha} d\boldsymbol{a} \\
&\qquad + \eta \iint_{\Omega\times\Omega_{\mathrm{TJ}}} \nabla_{\boldsymbol{a}} E \cdot \nabla_{\boldsymbol{a}} \phi g \exp\left(-\frac{E}{D}\right) d\Delta\boldsymbol{\alpha} d\boldsymbol{a}. \qquad (3.26)
\end{aligned}$$

From the fluctuation–dissipation relation (2.19), $3\gamma D = \frac{\beta^2_{\Delta\boldsymbol{\alpha}}}{2}$ and $\eta D = \frac{\beta^2_{\boldsymbol{a}}}{2}$, we have that

$$\begin{aligned}
&3\gamma D \iint_{\Omega\times\Omega_{\mathrm{TJ}}} \nabla^{\Omega}_{\Delta\boldsymbol{\alpha}} \phi \cdot \nabla^{\Omega}_{\Delta\boldsymbol{\alpha}} \left(g \exp\left(-\frac{E}{D}\right)\right) d\Delta\boldsymbol{\alpha} d\boldsymbol{a} \\
&\quad + \eta D \iint_{\Omega\times\Omega_{\mathrm{TJ}}} \nabla_{\boldsymbol{a}} \phi \cdot \nabla_{\boldsymbol{a}} \left(g \exp\left(-\frac{E}{D}\right)\right) d\Delta\boldsymbol{\alpha} d\boldsymbol{a} \\
&\quad + 3\gamma \iint_{\Omega\times\Omega_{\mathrm{TJ}}} \nabla^{\Omega}_{\Delta\boldsymbol{\alpha}} E \cdot \nabla^{\Omega}_{\Delta\boldsymbol{\alpha}} \phi g \exp\left(-\frac{E}{D}\right) d\Delta\boldsymbol{\alpha} d\boldsymbol{a} \\
&\quad + \eta \iint_{\Omega\times\Omega_{\mathrm{TJ}}} \nabla_{\boldsymbol{a}} E \cdot \nabla_{\boldsymbol{a}} \phi g \exp\left(-\frac{E}{D}\right) d\Delta\boldsymbol{\alpha} d\boldsymbol{a}
\end{aligned}$$

$$= \frac{\beta_{\Delta\boldsymbol{\alpha}}^2}{2} \iint_{\Omega\times\Omega_{\mathrm{TJ}}} \nabla_{\Delta\boldsymbol{\alpha}}^{\Omega}\phi \cdot \nabla_{\Delta\boldsymbol{\alpha}}^{\Omega} f \, d\Delta\boldsymbol{\alpha} d\boldsymbol{a} + \frac{\beta_{\boldsymbol{a}}^2}{2} \iint_{\Omega\times\Omega_{\mathrm{TJ}}} \nabla_{\boldsymbol{a}}\phi \cdot \nabla_{\boldsymbol{a}} f \, d\Delta\boldsymbol{\alpha} d\boldsymbol{a}$$
$$- \iint_{\Omega\times\Omega_{\mathrm{TJ}}} \boldsymbol{v}_{\Delta\boldsymbol{\alpha}} \cdot \nabla_{\Delta\boldsymbol{\alpha}}^{\Omega}\phi f \, d\Delta\boldsymbol{\alpha} d\boldsymbol{a} - \iint_{\Omega\times\Omega_{\mathrm{TJ}}} \boldsymbol{v}_{\boldsymbol{a}} \cdot \nabla_{\boldsymbol{a}}\phi f \, d\Delta\boldsymbol{\alpha} d\boldsymbol{a}, \tag{3.27}$$

where we used $\boldsymbol{v}_{\Delta\boldsymbol{\alpha}} = -3\gamma\nabla_{\Delta\boldsymbol{\alpha}}^{\Omega} E$, $\boldsymbol{v}_{\boldsymbol{a}} = -\eta\nabla_{\boldsymbol{a}} E$, and $f = g\exp(-E/D)$, (3.7). Plugging (3.26), (3.27), and $f = g\exp(-E/D)$ again into (3.25), we obtain that f is a weak solution (3.9) to (3.1). □

3.2. *Exponential decay of f*

We study the long-time asymptotics of the solution f of the Fokker–Planck equation (3.1). In order to derive that f converges to f_∞ (3.5), we will show that $g = f\exp(E/D)$ converges to some constant. Hereafter, we assume the 2-Poincaré–Wirtinger inequality on $\Omega\times\Omega_{\mathrm{TJ}}$, that is, there exists a positive constant $C_3 > 0$ such that for $g \in C^\infty(\Omega\times\Omega_{\mathrm{TJ}})$,

$$\iint_{\Omega\times\Omega_{\mathrm{TJ}}} |g - \bar{g}|^2 \, d\Delta\boldsymbol{\alpha} d\boldsymbol{a} \le C_3 \iint_{\Omega\times\Omega_{\mathrm{TJ}}} \left(|\nabla_{\Delta\boldsymbol{\alpha}}^{\Omega} g|^2 + |\nabla_{\boldsymbol{a}} g|^2\right) \, d\Delta\boldsymbol{\alpha} d\boldsymbol{a}, \tag{3.28}$$

where

$$\bar{g} = \frac{1}{|\Omega\times\Omega_{\mathrm{TJ}}|} \iint_{\Omega\times\Omega_{\mathrm{TJ}}} g \, d\Delta\boldsymbol{\alpha} d\boldsymbol{a} \tag{3.29}$$

is the integral mean on $\Omega\times\Omega_{\mathrm{TJ}}$. For example, when Ω is a bounded convex domain, 2-Poincaré–Wirtinger inequality (3.28) holds (see Ref. 35, Lemma 6.12).

We now show that $\Omega\times\Omega_{\mathrm{TJ}}$ supports the 2-Poincaré–Wirtinger inequality (3.28) in the weighted L^2 space $L^2(\Omega\times\Omega_{\mathrm{TJ}}, dm)$.

Lemma 3.4. *Assume* (3.28) *holds. Then, there exists* $C_4 > 0$ *such that for* $g \in C^\infty(\Omega\times\Omega_{\mathrm{TJ}})$, *we have that*

$$\|g - \bar{g}_{L^2(\Omega\times\Omega_{\mathrm{TJ}}, dm)}\|_{L^2(\Omega\times\Omega_{\mathrm{TJ}}, dm)}^2 \le C_4 \iint_{\Omega\times\Omega_{\mathrm{TJ}}} \left(|\nabla_{\Delta\boldsymbol{\alpha}}^{\Omega} g|^2 + |\nabla_{\boldsymbol{a}} g|^2\right) \, dm, \tag{3.30}$$

where a constant C_1 *is defined in* (3.6) *and*

$$\bar{g}_{L^2(\Omega\times\Omega_{\mathrm{TJ}}, dm)} = C_1 \iint_{\Omega\times\Omega_{\mathrm{TJ}}} g \, dm. \tag{3.31}$$

Proof. First, we notice that for $g \in C^\infty(\Omega\times\Omega_{\mathrm{TJ}})$,

$$\iint_{\Omega\times\Omega_{\mathrm{TJ}}} |g - \bar{g}_{L^2(\Omega\times\Omega_{\mathrm{TJ}}, dm)}|^2 \, dm = \inf_{\lambda\in\mathbb{R}} \iint_{\Omega\times\Omega_{\mathrm{TJ}}} |g - \lambda|^2 \, dm. \tag{3.32}$$

This is because, by (3.6), the quadratic form

$$\iint_{\Omega\times\Omega_{\mathrm{TJ}}} |g-\lambda|^2\,dm = \lambda^2 \iint_{\Omega\times\Omega_{\mathrm{TJ}}} dm - 2\lambda \iint_{\Omega\times\Omega_{\mathrm{TJ}}} g\,dm + \iint_{\Omega\times\Omega_{\mathrm{TJ}}} g^2\,dm$$
$$= \frac{\lambda^2}{C_1} - 2\lambda \iint_{\Omega\times\Omega_{\mathrm{TJ}}} g\,dm + \iint_{\Omega\times\Omega_{\mathrm{TJ}}} g^2\,dm, \tag{3.33}$$

is minimized at $\lambda = \bar{g}_{L^2(\Omega\times\Omega_{\mathrm{TJ}},dm)}$. Thus, taking λ as $\bar{g}$, we have

$$\iint_{\Omega\times\Omega_{\mathrm{TJ}}} |g-\bar{g}_{L^2(\Omega\times\Omega_{\mathrm{TJ}},dm)}|^2\,dm \le \iint_{\Omega\times\Omega_{\mathrm{TJ}}} |g-\bar{g}|^2\,dm. \tag{3.34}$$

Next, we let

$$C_5 = \inf_{(\Delta\boldsymbol{\alpha},\boldsymbol{\alpha})} e^{-\frac{E(\Delta\boldsymbol{\alpha},\boldsymbol{a})}{D}}, \quad C_6 = \sup_{(\Delta\boldsymbol{\alpha},\boldsymbol{\alpha})} e^{-\frac{E(\Delta\boldsymbol{\alpha},\boldsymbol{a})}{D}}, \tag{3.35}$$

so that $C_5 \le e^{-\frac{E}{D}} \le C_6$ on $\Omega\times\Omega_{\mathrm{TJ}}$. Then, $C_5 d\Delta\boldsymbol{\alpha} d\boldsymbol{a} \le dm \le C_6 d\Delta\boldsymbol{\alpha} d\boldsymbol{a}$, hence

$$\|g-\bar{g}_{L^2(\Omega\times\Omega_{\mathrm{TJ}},dm)}\|^2_{L^2(\Omega\times\Omega_{\mathrm{TJ}},dm)} \le \iint_{\Omega\times\Omega_{\mathrm{TJ}}} |g-\bar{g}|^2\,dm$$
$$\le C_6 \iint_{\Omega\times\Omega_{\mathrm{TJ}}} |g-\bar{g}|^2\,d\Delta\boldsymbol{\alpha} d\boldsymbol{a}. \tag{3.36}$$

Next, we use the 2-Poincaré–Wirtinger inequality (3.28) and $C_5 d\Delta\boldsymbol{\alpha} d\boldsymbol{a} \le dm$, then we obtain

$$\|g-\bar{g}_{L^2(\Omega\times\Omega_{\mathrm{TJ}},dm)}\|^2_{L^2(\Omega\times\Omega_{\mathrm{TJ}},dm)} \le C_6 \iint_{\Omega\times\Omega_{\mathrm{TJ}}} |g-\bar{g}|^2\,d\Delta\boldsymbol{\alpha} d\boldsymbol{a}$$
$$\le C_6 C_3 \iint_{\Omega\times\Omega_{\mathrm{TJ}}} \left(|\nabla^{\Omega}_{\Delta\boldsymbol{\alpha}} g|^2 + |\nabla_{\boldsymbol{a}} g|^2\right)\,d\Delta\boldsymbol{\alpha} d\boldsymbol{a}$$
$$\le \frac{C_6 C_3}{C_5} \iint_{\Omega\times\Omega_{\mathrm{TJ}}} \left(|\nabla^{\Omega}_{\Delta\boldsymbol{\alpha}} g|^2 + |\nabla_{\boldsymbol{a}} g|^2\right)\,dm. \tag{3.37}$$

Therefore, the inequality (3.30) holds for

$$C_4 = \frac{C_6 C_3}{C_5}. \tag{3.38}$$

□

Now we are in position to derive the long-time asymptotic behavior for the solution of the Fokker–Planck equation (3.1).

Theorem 3.1. *Assume that σ is a C^1 function on $\mathbb{R}$ and $\Omega\times\Omega_{\mathrm{TJ}}$ supports the 2-Poincaré–Wirtinger inequality* (3.28). *Let $f_0 \in L^2(\Omega\times\Omega_{\mathrm{TJ}}, e^{\frac{E}{D}} d\Delta\boldsymbol{\alpha} d\boldsymbol{a})$ be a probability density function. Then, there exists a constant $C_7 > 0$ such that the*

associated solution f of (3.1) *satisfies*

$$\iint_{\Omega\times\Omega_{\mathrm{TJ}}} |f(\Delta\boldsymbol{\alpha},\boldsymbol{a},t)-f_\infty(\Delta\boldsymbol{\alpha},\boldsymbol{a})|^2\exp\left(\frac{E(\Delta\boldsymbol{\alpha},\boldsymbol{a})}{D}\right)d\Delta\boldsymbol{\alpha}d\boldsymbol{a}$$
$$\le C_7 e^{-\frac{2\min\{3\gamma,\eta\}D}{C_4}t} \tag{3.39}$$

for $t>0$, where f_∞, C_1, and C_4 are defined in (3.5), (3.6), *and* (3.38), *respectively.*

Proof. We multiply (3.24) by $(g-\bar{g}_{L^2(\Omega\times\Omega_{\mathrm{TJ}},dm)})\exp(-\frac{E}{D})$ and integrate over $\Omega\times\Omega_{\mathrm{TJ}}$. Since $\bar{g}_{L^2(\Omega\times\Omega_{\mathrm{TJ}},dm)}$ and $\exp(-\frac{E}{D})$ are independent of t, we obtain that

$$\frac{1}{2}\frac{d}{dt}\iint_{\Omega\times\Omega_{\mathrm{TJ}}}|g-\bar{g}_{L^2(\Omega\times\Omega_{\mathrm{TJ}},dm)}|^2\,dm=(Lg,g-\bar{g}_{L^2(\Omega\times\Omega_{\mathrm{TJ}},dm)})_{L^2(\Omega\times\Omega_{\mathrm{TJ}},dm)}.$$

By (3.23) we get

$$(Lg,g-\bar{g}_{L^2(\Omega\times\Omega_{\mathrm{TJ}},dm)})_{L^2(\Omega\times\Omega_{\mathrm{TJ}},dm)}$$
$$=-3\gamma D\iint_{\Omega\times\Omega_{\mathrm{TJ}}}|\nabla^{\Omega}_{\Delta\boldsymbol{\alpha}}g|^2\,dm-\eta D\iint_{\Omega\times\Omega_{\mathrm{TJ}}}|\nabla_{\boldsymbol{a}}g|^2\,dm.$$

Combining the above relations with the Poincaré inequality (3.30), we have that,

$$\frac{1}{2}\frac{d}{dt}\iint_{\Omega\times\Omega_{\mathrm{TJ}}}|g-\bar{g}_{L^2(\Omega\times\Omega_{\mathrm{TJ}},dm)}|^2\,dm$$
$$\le-\frac{\min\{3\gamma,\eta\}D}{C_4}\|g-\bar{g}_{L^2(\Omega\times\Omega_{\mathrm{TJ}},dm)}\|^2_{L^2(\Omega\times\Omega_{\mathrm{TJ}},dm)}. \tag{3.40}$$

Therefore, by Gronwall's inequality, we deduce that

$$\iint_{\Omega\times\Omega_{\mathrm{TJ}}}|g-\bar{g}_{L^2(\Omega\times\Omega_{\mathrm{TJ}},dm)}|^2\,dm$$
$$\le e^{-2\frac{\min\{3\gamma,\eta\}D}{C_4}t}\iint_{\Omega\times\Omega_{\mathrm{TJ}}}|g_0-\bar{g}_{L^2(\Omega\times\Omega_{\mathrm{TJ}},dm)}|^2\,dm$$
$$=:C_7e^{-\frac{2\min\{3\gamma,\eta\}D}{C_4}t}, \tag{3.41}$$

where $g_0=f_0\exp(-E/D)$. Using that, $g=f\exp(E/D)$, we have

$$\iint_{\Omega\times\Omega_{\mathrm{TJ}}}|g-\bar{g}_{L^2(\Omega\times\Omega_{\mathrm{TJ}},dm)}|^2\,dm$$
$$=\iint_{\Omega\times\Omega_{\mathrm{TJ}}}\left|f-\bar{g}_{L^2(\Omega\times\Omega_{\mathrm{TJ}},dm)}\exp\left(-\frac{E}{D}\right)\right|^2\exp\left(\frac{E}{D}\right)d\Delta\boldsymbol{\alpha}d\boldsymbol{a}. \tag{3.42}$$

Integrating (3.1) on $\Omega\times\Omega_{\mathrm{TJ}}$, applying the integration by parts and using boundary conditions (3.1), we obtain that

$$\frac{d}{dt}\iint_{\Omega\times\Omega_{\mathrm{TJ}}}f\,d\Delta\boldsymbol{\alpha}d\boldsymbol{a}=\iint_{\Omega\times\Omega_{\mathrm{TJ}}}\frac{\partial f}{\partial t}\,d\Delta\boldsymbol{\alpha}d\boldsymbol{a}=0. \tag{3.43}$$

Hence, due to the assumption on the initial data (3.4), it follows that

$$\iint_{\Omega\times\Omega_{\mathrm{TJ}}} f(t,\Delta\boldsymbol{\alpha},\boldsymbol{a})\,d\Delta\boldsymbol{\alpha}d\boldsymbol{a} = \iint_{\Omega\times\Omega_{\mathrm{TJ}}} f_0(\Delta\boldsymbol{\alpha},\boldsymbol{a})\,d\Delta\boldsymbol{\alpha}d\boldsymbol{a} = 1,$$

for $t>0$. Since, $f = g\exp(-E/D)$ and $dm = \exp(-E/D)d\Delta\boldsymbol{\alpha}d\boldsymbol{a}$, we have that

$$\bar{g}_{L^2(\Omega\times\Omega_{\mathrm{TJ}},dm)} = C_1\iint_{\Omega\times\Omega_{\mathrm{TJ}}} g\,dm = C_1\iint_{\Omega\times\Omega_{\mathrm{TJ}}} f\,d\Delta\boldsymbol{\alpha}d\boldsymbol{a} = C_1. \tag{3.44}$$

Combining (3.41), (3.44) and $f_\infty = C_1\exp(-E/D)$, we obtain (3.39). □

3.3. *Exponential decay for f_t*

Next, we study finer asymptotics of the solution f of the Fokker–Planck equation (3.1). Due to the properties of self-adjointness of L, the solution f is smooth in time even though f may not be smooth in space. Thus, we consider long-time asymptotic behavior of f_t.

Theorem 3.2. *Assume that σ is a C^1 function on $\mathbb{R}$ and $\Omega\times\Omega_{\mathrm{TJ}}$ supports the 2-Poincaré–Wirtinger inequality* (3.28). *Let $f_0\in L^2(\Omega\times\Omega_{\mathrm{TJ}}, e^{\frac{E}{D}}\,d\Delta\boldsymbol{\alpha}d\boldsymbol{a})$ be a probability density function. Then, for any $t_0>0$, there exists a constant $C_8>0$, such that the associated solution f of* (3.1) *satisfies*

$$\iint_{\Omega\times\Omega_{\mathrm{TJ}}} |f_t(\Delta\boldsymbol{\alpha},\boldsymbol{a},t)|^2\exp\left(\frac{E(\Delta\boldsymbol{\alpha},\boldsymbol{a})}{D}\right)d\Delta\boldsymbol{\alpha}d\boldsymbol{a} \le C_8 e^{-\frac{2\min\{3\gamma,\eta\}D}{C_4}t} \tag{3.45}$$

for $t>t_0$, where C_4 is a constant defined in (3.38).

Proof. The equation $g_t = Lg$, (3.16) can be written as

$$\begin{aligned}\exp\left(-\frac{E}{D}\right)g_t = {}& 3\gamma D\nabla^{\Omega}_{\Delta\boldsymbol{\alpha}}\cdot\left(\exp\left(-\frac{E}{D}\right)\nabla^{\Omega}_{\Delta\boldsymbol{\alpha}}g\right)\\ &+\eta D\nabla_{\boldsymbol{a}}\cdot\left(\exp\left(-\frac{E}{D}\right)\nabla_{\boldsymbol{a}}g\right).\end{aligned} \tag{3.46}$$

Note that $E(\Delta\boldsymbol{\alpha},\boldsymbol{a})$ is a function of only misorientations and the positions of the triple junctions. Take a derivative in time of (3.46), then,

$$\begin{aligned}\exp\left(-\frac{E}{D}\right)g_{tt} = {}& 3\gamma D\nabla^{\Omega}_{\Delta\boldsymbol{\alpha}}\cdot\left(\exp\left(-\frac{E}{D}\right)\nabla^{\Omega}_{\Delta\boldsymbol{\alpha}}g_t\right)\\ &+\eta D\nabla_{\boldsymbol{a}}\cdot\left(\exp\left(-\frac{E}{D}\right)\nabla_{\boldsymbol{a}}g_t\right).\end{aligned} \tag{3.47}$$

Multiplying (3.47) by g_t, integrating over $\Omega\times\Omega_{\mathrm{TJ}}$, integrating by parts and using the boundary conditions (3.19), it follows that

$$\frac{1}{2}\frac{d}{dt}\iint_{\Omega\times\Omega_{\mathrm{TJ}}}|g_t|^2\,dm = -\iint_{\Omega\times\Omega_{\mathrm{TJ}}}\left(3\gamma D|\nabla^{\Omega}_{\Delta\boldsymbol{\alpha}}g_t|^2+\eta D|\nabla_{\boldsymbol{a}}g_t|^2\right)dm. \tag{3.48}$$

Next, note that

$$\iint_{\Omega\times\Omega_{\mathrm{TJ}}} g_t \, dm = 0,$$

thus, we obtain by the Poincaré inequality

$$\iint_{\Omega\times\Omega_{\mathrm{TJ}}} \left(3\gamma D|\nabla^{\Omega}_{\Delta\boldsymbol{\alpha}} g_t|^2 + \eta D|\nabla_{\boldsymbol{a}} g_t|^2\right) \, dm \geq \frac{\min\{3\gamma,\eta\}}{C_4} \iint_{\Omega\times\Omega_{\mathrm{TJ}}} |g_t|^2 \, dm.$$

Hence, one can obtain from (3.48) that

$$\frac{1}{2}\frac{d}{dt}\iint_{\Omega\times\Omega_{\mathrm{TJ}}} |g_t|^2 \, dm \leq -\frac{\min\{3\gamma,\eta\}}{C_4} \iint_{\Omega\times\Omega_{\mathrm{TJ}}} |g_t|^2 \, dm.$$

Thus, by Gronwall's inequality,

$$\begin{aligned}\iint_{\Omega\times\Omega_{\mathrm{TJ}}} |g_t(\Delta\boldsymbol{\alpha},\boldsymbol{a},t)|^2 \, dm \;&\leq\; \left(\iint_{\Omega\times\Omega_{\mathrm{TJ}}} |g_t(\Delta\boldsymbol{\alpha},\boldsymbol{a},t_0)|^2 \, dm\right) e^{-\frac{2\min\{3\gamma,\eta\}D}{C_4}t} \\ &=: C_8 e^{-\frac{2\min\{3\gamma,\eta\}D}{C_4}t}. \end{aligned} \tag{3.49}$$

for $t > t_0$. Note again, that $f = g\exp(-E/D)$, $dm = \exp(-E/D)\, d\Delta\boldsymbol{\alpha} d\boldsymbol{a}$, and,

$$\iint_{\Omega\times\Omega_{\mathrm{TJ}}} |g_t|^2 \, dm = \iint_{\Omega\times\Omega_{\mathrm{TJ}}} |f_t|^2 \exp\left(\frac{E}{D}\right) \, d\Delta\boldsymbol{\alpha} d\boldsymbol{a}. \tag{3.50}$$

Therefore, the estimate (3.45) follows. □

3.4. *Exponential decay for the gradient of f*

Here we establish the exponential decay for the gradient of f. To derive the asymptotics of the gradient of f, one may consider the equation for the derivative of f. However, we cannot take a space derivative of the Fokker–Planck equation (3.1), because of lack of regularity for the solution f. Nevertheless, from the exponential decay for f_t in Theorem 3.2, one can obtain a long time asymptotics for the gradient of f.

Theorem 3.3. *Assume that σ is a C^1 function on $\mathbb{R}$ and $\Omega\times\Omega_{\mathrm{TJ}}$ supports the 2-Poincaré–Wirtinger inequality* (3.28)*. Let $f_0 \in L^2(\Omega\times\Omega_{\mathrm{TJ}}, e^{\frac{E}{D}}\, d\Delta\boldsymbol{\alpha} d\boldsymbol{a})$ be a probability density function. Then, for any $t_0 > 0$, there is a constant $C_9 > 0$, such that the associated solution f of* (3.1) *satisfies,*

$$\begin{aligned}&\iint_{\Omega\times\Omega_{\mathrm{TJ}}} \left(3\gamma D|\nabla^{\Omega}_{\Delta\boldsymbol{\alpha}}(f-f_\infty)|^2 + \eta D|\nabla_{\boldsymbol{a}}(f-f_\infty)|^2\right)\exp\left(\frac{E(\Delta\boldsymbol{\alpha},\boldsymbol{a})}{D}\right) \, d\Delta\boldsymbol{\alpha} d\boldsymbol{a} \\ &\quad\leq C_9 e^{-\frac{2\min\{3\gamma,\eta\}D}{C_4}t}\end{aligned} \tag{3.51}$$

for $t > t_0$, where C_4 is a constant (3.38)*.*

Proof. Multiplying (3.46) by g_t, integrating over $\Omega\times\Omega_{\mathrm{TJ}}$, and using the integration by parts with the boundary conditions (3.19), one can show

$$\begin{aligned}
&\iint_{\Omega\times\Omega_{\mathrm{TJ}}} |g_t|^2\,dm\\
&\quad= \iint_{\Omega\times\Omega_{\mathrm{TJ}}} \left(3\gamma D\nabla^{\Omega}_{\Delta\boldsymbol{\alpha}}\cdot\left(\exp\left(-\frac{E}{D}\right)\nabla^{\Omega}_{\Delta\boldsymbol{\alpha}}g\right)\right.\\
&\qquad\left.+\eta D\nabla_{\boldsymbol{a}}\cdot\left(\exp\left(-\frac{E}{D}\right)\nabla_{\boldsymbol{a}}g\right)\right)g_t\,d\Delta\boldsymbol{\alpha}d\boldsymbol{a}\\
&\quad= -\iint_{\Omega\times\Omega_{\mathrm{TJ}}} \left(3\gamma D\left(\exp\left(-\frac{E}{D}\right)\nabla^{\Omega}_{\Delta\boldsymbol{\alpha}}g\right)\cdot\nabla^{\Omega}_{\Delta\boldsymbol{\alpha}}g_t\right.\\
&\qquad\left.+\eta D\left(\exp\left(-\frac{E}{D}\right)\nabla_{\boldsymbol{a}}g\right)\cdot\nabla_{\boldsymbol{a}}g_t\right)d\Delta\boldsymbol{\alpha}d\boldsymbol{a}. \qquad (3.52)
\end{aligned}$$

On the other hand, by direct computation and $dm = e^{-E/D}\,d\Delta\boldsymbol{\alpha}d\boldsymbol{a}$, we have

$$\begin{aligned}
&\frac{1}{2}\frac{d}{dt}\iint_{\Omega\times\Omega_{\mathrm{TJ}}}\left(3\gamma D|\nabla^{\Omega}_{\Delta\boldsymbol{\alpha}}g|^2+\eta D|\nabla_{\boldsymbol{a}}g|^2\right)dm\\
&\quad= \iint_{\Omega\times\Omega_{\mathrm{TJ}}} \left(3\gamma D\left(\exp\left(-\frac{E}{D}\right)\nabla^{\Omega}_{\Delta\boldsymbol{\alpha}}g\right)\cdot\nabla^{\Omega}_{\Delta\boldsymbol{\alpha}}g_t\right.\\
&\qquad\left.+\eta D\left(\exp\left(-\frac{E}{D}\right)\nabla_{\boldsymbol{a}}g\right)\cdot\nabla_{\boldsymbol{a}}g_t\right)d\Delta\boldsymbol{\alpha}d\boldsymbol{a}.
\end{aligned}$$

Thus, we arrive at

$$\iint_{\Omega\times\Omega_{\mathrm{TJ}}}|g_t|^2\,dm = -\frac{1}{2}\frac{d}{dt}\iint_{\Omega\times\Omega_{\mathrm{TJ}}}\left(3\gamma D|\nabla^{\Omega}_{\Delta\boldsymbol{\alpha}}g|^2+\eta D|\nabla_{\boldsymbol{a}}g|^2\right)dm.$$

Using (3.49) and non-negativity of the integral of $|g_t|^2$, one can obtain, for $t > t_0$,

$$-2C_8e^{-\frac{2\min\{3\gamma,\eta\}D}{C_4}t} \le \frac{d}{dt}\iint_{\Omega\times\Omega_{\mathrm{TJ}}}\left(3\gamma D|\nabla^{\Omega}_{\Delta\boldsymbol{\alpha}}g|^2+\eta D|\nabla_{\boldsymbol{a}}g|^2\right)dm \le 0. \qquad (3.53)$$

Specifically, $3\gamma D\|\nabla^{\Omega}_{\Delta\boldsymbol{\alpha}}g\|^2_{L^2(\Omega\times\Omega_{\mathrm{TJ}},dm)} + \eta D\|\nabla_{\boldsymbol{a}}g\|^2_{L^2(\Omega\times\Omega_{\mathrm{TJ}},dm)}$ is monotone decreasing in time. On the other hand, multiplying (3.46) by g, integrating by parts and using the boundary conditions (3.19), we have

$$\frac{d}{dt}\iint_{\Omega\times\Omega_{\mathrm{TJ}}}|g|^2\,dm + \iint_{\Omega\times\Omega_{\mathrm{TJ}}}\left(3\gamma D|\nabla^{\Omega}_{\Delta\boldsymbol{\alpha}}g|^2+\eta D|\nabla_{\boldsymbol{a}}g|^2\right)dm = 0. \qquad (3.54)$$

Now, integrating over $0 \le t \le T$ for $T > 0$, we arrive at

$$\begin{aligned}
&\iint_{\Omega\times\Omega_{\mathrm{TJ}}}|g|^2\,dm\Big|_{t=T} + \int_0^T dt\iint_{\Omega\times\Omega_{\mathrm{TJ}}}\left(3\gamma D|\nabla^{\Omega}_{\Delta\boldsymbol{\alpha}}g|^2+\eta D|\nabla_{\boldsymbol{a}}g|^2\right)dm\\
&\quad= \iint_{\Omega\times\Omega_{\mathrm{TJ}}}|g|^2\,dm\Big|_{t=0}. \qquad (3.55)
\end{aligned}$$

Thus, there is a positive monotone increasing sequence $\{t_j\}$ such that $t_j \to \infty$ and

$$\iint_{\Omega\times\Omega_{\mathrm{TJ}}} \left(3\gamma D|\nabla^{\Omega}_{\Delta\boldsymbol{\alpha}} g|^2 + \eta D|\nabla_{\boldsymbol{a}} g|^2\right)\, dm\Big|_{t=t_j} \to 0 \quad \text{as } t_j \to \infty. \tag{3.56}$$

Using the monotonicity in time of $3\gamma D\|\nabla^{\Omega}_{\Delta\boldsymbol{\alpha}} g\|^2_{L^2(\Omega\times\Omega_{\mathrm{TJ}},dm)} + \eta D\|\nabla_{\boldsymbol{a}} g\|^2_{L^2(\Omega\times\Omega_{\mathrm{TJ}},dm)}$, we can take a full limit in time of (3.56), namely

$$\iint_{\Omega\times\Omega_{\mathrm{TJ}}} \left(3\gamma D|\nabla^{\Omega}_{\Delta\boldsymbol{\alpha}} g|^2 + \eta D|\nabla_{\boldsymbol{a}} g|^2\right)\, dm \to 0 \quad \text{as } t \to \infty. \tag{3.57}$$

Next, for $0 < T < T'$, we obtain

$$\begin{aligned}
&\left|\iint_{\Omega\times\Omega_{\mathrm{TJ}}} \left(3\gamma D|\nabla^{\Omega}_{\Delta\boldsymbol{\alpha}} g|^2 + \eta D|\nabla_{\boldsymbol{a}} g|^2\right)\, dm\Big|_{t=T'}\right. \\
&\qquad \left. - \iint_{\Omega\times\Omega_{\mathrm{TJ}}} \left(3\gamma D|\nabla^{\Omega}_{\Delta\boldsymbol{\alpha}} g|^2 + \eta D|\nabla_{\boldsymbol{a}} g|^2\right)\, dm\Big|_{t=T}\right| \\
&= \left|\int_T^{T'} \left(\frac{d}{dt}\iint_{\Omega\times\Omega_{\mathrm{TJ}}} \left(3\gamma D|\nabla^{\Omega}_{\Delta\boldsymbol{\alpha}} g|^2 + \eta D|\nabla_{\boldsymbol{a}} g|^2\right)\, dm\right)\, dt\right| \\
&\le \int_T^{T'} \left|\frac{d}{dt}\iint_{\Omega\times\Omega_{\mathrm{TJ}}} \left(3\gamma D|\nabla^{\Omega}_{\Delta\boldsymbol{\alpha}} g|^2 + \eta D|\nabla_{\boldsymbol{a}} g|^2\right)\, dm\right|\, dt.
\end{aligned} \tag{3.58}$$

Using (3.53), we deduce

$$\left|\frac{d}{dt}\iint_{\Omega\times\Omega_{\mathrm{TJ}}} \left(3\gamma D|\nabla^{\Omega}_{\Delta\boldsymbol{\alpha}} g|^2 + \eta D|\nabla_{\boldsymbol{a}} g|^2\right)\, dm\right| \le 2C_8 e^{-\frac{2\min\{3\gamma,\eta\}D}{C_4}t}.$$

Hence, we arrive at

$$\begin{aligned}
&\left|\iint_{\Omega\times\Omega_{\mathrm{TJ}}} \left(3\gamma D|\nabla^{\Omega}_{\Delta\boldsymbol{\alpha}} g|^2 + \eta D|\nabla_{\boldsymbol{a}} g|^2\right)\, dm\Big|_{t=T'}\right. \\
&\qquad \left. - \iint_{\Omega\times\Omega_{\mathrm{TJ}}} \left(3\gamma D|\nabla^{\Omega}_{\Delta\boldsymbol{\alpha}} g|^2 + \eta D|\nabla_{\boldsymbol{a}} g|^2\right)\, dm\Big|_{t=T}\right| \\
&\le \int_T^{T'} 2C_8 e^{-\frac{2\min\{3\gamma,\eta\}D}{C_4}t}\, dt \\
&= \frac{C_8C_4}{\min\{3\gamma,\eta\}D}\left(e^{-\frac{2\min\{3\gamma,\eta\}D}{C_4}T} - e^{-\frac{2\min\{3\gamma,\eta\}D}{C_4}T'}\right).
\end{aligned} \tag{3.59}$$

Taking a limit $T' \to \infty$, we obtain that

$$\iint_{\Omega\times\Omega_{\mathrm{TJ}}} \left(3\gamma D|\nabla^{\Omega}_{\Delta\boldsymbol{\alpha}} g|^2 + \eta D|\nabla_{\boldsymbol{a}} g|^2\right)\, dm\Big|_{t=T} \le \frac{C_8C_4}{\min\{3\gamma,\eta\}D} e^{-\frac{2\min\{3\gamma,\eta\}D}{C_4}T}. \tag{3.60}$$

In addition, by direct calculation, we have that

$$\begin{aligned}\nabla(f-f_\infty) &= \left(\nabla g - \frac{1}{D}(g-C_1)\nabla E\right)\exp\left(-\frac{E}{D}\right)\\ &= \nabla g \exp\left(-\frac{E}{D}\right) - \frac{1}{D}(f-f_\infty)\nabla E,\end{aligned}$$

where ∇ is $\nabla^{\Omega}_{\Delta\boldsymbol{\alpha}}$ or $\nabla_{\boldsymbol{a}}$. Thus,

$$\begin{aligned}&\iint_{\Omega\times\Omega_{\mathrm{TJ}}} |\nabla^{\Omega}_{\Delta\boldsymbol{\alpha}}(f-f_\infty)|^2 \exp\left(\frac{E}{D}\right) d\Delta\boldsymbol{\alpha} d\boldsymbol{a}\\ &\quad\le 2\iint_{\Omega\times\Omega_{\mathrm{TJ}}} |\nabla^{\Omega}_{\Delta\boldsymbol{\alpha}} g|^2 \exp\left(-\frac{E}{D}\right) d\Delta\boldsymbol{\alpha} d\boldsymbol{a}\\ &\qquad + \frac{2}{D^2}\iint_{\Omega\times\Omega_{\mathrm{TJ}}} |f-f_\infty|^2 |\nabla^{\Omega}_{\Delta\boldsymbol{\alpha}} E|^2 \exp\left(\frac{E}{D}\right) d\Delta\boldsymbol{\alpha} d\boldsymbol{a}.\end{aligned}$$

Therefore, from (3.39), (3.60), and boundedness of the gradient of E, there is a constant $C_{10}>0$, such that

$$\iint_{\Omega\times\Omega_{\mathrm{TJ}}} |\nabla^{\Omega}_{\Delta\boldsymbol{\alpha}}(f-f_\infty)|^2 \exp\left(\frac{E}{D}\right) d\Delta\boldsymbol{\alpha} d\boldsymbol{a} \le C_{10} e^{-\frac{2\min\{3\gamma,\eta\}D}{C_4}t}.$$

Similarly, there is a constant $C_{11}>0$ such that

$$\iint_{\Omega\times\Omega_{\mathrm{TJ}}} |\nabla_{\boldsymbol{a}}(f-f_\infty)|^2 \exp\left(\frac{E}{D}\right) d\Delta\boldsymbol{\alpha} d\boldsymbol{a} \le C_{11} e^{-\frac{2\min\{3\gamma,\eta\}D}{C_4}t},$$

hence, we obtain (3.51). □

Remark 3.1. Since E is not C^2 for $\boldsymbol{a}\in\Omega_{\mathrm{TJ}}$, it is not known that g is in C^3 on Ω_{TJ}, hence one cannot take a derivative in $\boldsymbol{a}$ of (3.24). However, g is smooth in time so we can take a derivative in time. Note that, we do not use third derivative in $\boldsymbol{a}$ in the proof of Theorem 3.3 (cf. Refs. 34 and 43).

Remark 3.2. In Theorems 3.1–3.3, decay rate of solutions to (3.1) may not be optimal. It will be part of a future work to obtain optimal decay orders and dependence on the relaxation time scales $\gamma,\eta>0$.

Remark 3.3. In this paper, we have used the Poincaré inequality to obtain the large-time asymptotics of the solution in the weighted L^2 framework. The specific difficulties for our system are related to the fact that the potential $\nabla^{\Omega}_{\Delta\boldsymbol{\alpha}}E$ is degenerate and $\nabla_{\boldsymbol{a}}E$ is not smooth enough. When the potential has better properties, such as non-degeneracy and smoothness, one could try to employ the logarithmic-Sobolev inequality or the higher order energy estimates[1, 2, 27, 42] to obtain the results in weaker spaces. This is currently under study, and one of the subjects of our forthcoming work would be to study the logarithmic-Sobolev type of inequalities and

Bakry–Émery theory to construct the L^1 theory of the system discussed in this paper.

In this section, we obtained long-time asymptotics for joint distribution f on $\Omega \times \Omega_{\mathrm{TJ}}$ in the weighted L^2 space. In particular, we established that distribution f converges to the Boltzmann distribution $f_\infty(\Delta\boldsymbol{\alpha}, \boldsymbol{a}) = C_1 \exp(-\frac{E(\Delta\boldsymbol{\alpha},\boldsymbol{a})}{D})$ with respect to the grain boundary energy E on $\Omega \times \Omega_{\mathrm{TJ}}$. In the next section, we will study long-time asymptotics of the marginal probability density.

4. Marginal Probability Distribution

In this section, for a solution f of the Fokker–Planck equation (3.1), which is a joint distribution on $\Omega \times \Omega_{\mathrm{TJ}}$, we consider the marginal probability density of misorientations, ρ_1 of Ω. The probability density ρ_1 is related to the Grain Boundary Character Distribution (GBCD). The GBCD (in 2D context and with the grain boundary energy density which only depends on the misorientation $\Delta\alpha$) is an empirical statistical measure of the relative length (in 2D) of the grain boundary interface with a given lattice misorientation. GBCD can be viewed as a primary statistical descriptor to characterize texture of the grain boundary network, and is inversely related to the grain boundary energy density as discovered in experiments and simulations. The reader can consult, for instance, see Refs. 3, 5, 6 and 7 for more details about GBCD and the theory of the GBCD, and also Sec. 5.

In this section, we compare the long-time asymptotics for the marginal distribution $\rho_{1,\infty}$ and the Boltzmann distributions on Ω. Hence, let us define the marginal distributions for a misorientation $\Delta\boldsymbol{\alpha} = (\Delta\alpha^{(1)}, \Delta\alpha^{(2)}, \Delta\alpha^{(3)}) \in \Omega$, and for a position of the triple junction $\boldsymbol{a} \in \Omega_{\mathrm{TJ}}$,

$$\rho_1(\Delta\boldsymbol{\alpha}, t) = \int_{\Omega_{\mathrm{TJ}}} f(\Delta\boldsymbol{\alpha}, \boldsymbol{a}, t)\, d\boldsymbol{a}, \quad \rho_2(\boldsymbol{a}, t) = \int_{\Omega} f(\Delta\boldsymbol{\alpha}, \boldsymbol{a}, t)\, d\Delta\boldsymbol{\alpha}, \tag{4.1}$$

and

$$\rho_{1,\infty}(\Delta\boldsymbol{\alpha}) = \int_{\Omega_{\mathrm{TJ}}} f_\infty(\Delta\boldsymbol{\alpha}, \boldsymbol{a})\, d\boldsymbol{a}, \quad \rho_{2,\infty}(\boldsymbol{a}) = \int_{\Omega} f_\infty(\Delta\boldsymbol{\alpha}, \boldsymbol{a})\, d\Delta\boldsymbol{\alpha}. \tag{4.2}$$

From Theorems 3.1, 3.2, and 3.3 in Sec. 3, we can obtain long time asymptotics of ρ_1 and ρ_2.

Proposition 4.1. *Assume that σ is a C^1 function on $\mathbb{R}$ and $\Omega \times \Omega_{\mathrm{TJ}}$ supports the 2-Poincaré–Wirtinger inequality* (3.28). *Let $f_0 \in L^2(\Omega \times \Omega_{\mathrm{TJ}}, e^{\frac{E}{D}}\, d\Delta\boldsymbol{\alpha} d\boldsymbol{a})$ be a probability density function. Let ρ_1 be defined in* (4.1). *Then, for any $t_0 > 0$, there are positive constants C_{12}, C_{13}, and $C_{14} > 0$, such that for $t > t_0$,*

$$\int_{\Omega} |\rho_1(\Delta\boldsymbol{\alpha}, t) - \rho_{1,\infty}(\Delta\boldsymbol{\alpha})|^2\, d\Delta\boldsymbol{\alpha} \leq C_{12} e^{-\frac{2\min\{3\gamma,\eta\}D}{C_4} t},$$

$$\int_\Omega |(\rho_1)_t(\Delta\boldsymbol{\alpha},t)|^2\,d\Delta\boldsymbol{\alpha} \le C_{13}e^{-\frac{2\min\{3\gamma,\eta\}D}{C_4}t},$$
$$\int_\Omega |\nabla^\Omega_{\Delta\boldsymbol{\alpha}}(\rho_1(\Delta\boldsymbol{\alpha},t)-\rho_{1,\infty}(\Delta\boldsymbol{\alpha}))|^2\,d\Delta\boldsymbol{\alpha} \le C_{14}e^{-\frac{2\min\{3\gamma,\eta\}D}{C_4}t}, \tag{4.3}$$

where $C_4>0$ is a constant defined in (3.38).

Proof. We get by Hölder's inequality that,

$$|\rho_1(\Delta\boldsymbol{\alpha},t)-\rho_{1,\infty}(\Delta\boldsymbol{\alpha},t)|^2 = \left|\int_{\Omega_{\rm TJ}} (f(\Delta\boldsymbol{\alpha},\boldsymbol{a},t)-f_\infty(\Delta\boldsymbol{\alpha},\boldsymbol{a}))\,d\boldsymbol{a}\right|^2$$
$$\le |\Omega_{\rm TJ}|\int_{\Omega_{\rm TJ}} |f(\Delta\boldsymbol{\alpha},\boldsymbol{a},t)-f_\infty(\Delta\boldsymbol{\alpha},\boldsymbol{a})|^2\,d\boldsymbol{a}. \tag{4.4}$$

Next, note that $C_5 \le e^{-\frac{E}{D}} \le C_6$ on $\Omega\times\Omega_{\rm TJ}$, where the constants $C_5, C_6>0$ are defined in (3.35). Thus, we obtain

$$\int_{\Omega_{\rm TJ}} |f(\Delta\boldsymbol{\alpha},\boldsymbol{a},t)-f_\infty(\Delta\boldsymbol{\alpha},\boldsymbol{a})|^2\,d\boldsymbol{a}$$
$$\le C_6\int_{\Omega_{\rm TJ}} |f(\Delta\boldsymbol{\alpha},\boldsymbol{a},t)-f_\infty(\Delta\boldsymbol{\alpha},\boldsymbol{a})|^2 \exp\left(\frac{E(\Delta\boldsymbol{\alpha},\boldsymbol{a})}{D}\right)d\boldsymbol{a}. \tag{4.5}$$

Then, using (3.39), we have

$$\int_\Omega |\rho_1(\Delta\boldsymbol{\alpha},t)-\rho_{1,\infty}(\Delta\boldsymbol{\alpha},t)|^2\,d\Delta\boldsymbol{\alpha}$$
$$\le C_6|\Omega_{\rm TJ}|\iint_{\Omega\times\Omega_{\rm TJ}} |f(\Delta\boldsymbol{\alpha},\boldsymbol{a},t)-f_\infty(\Delta\boldsymbol{\alpha},\boldsymbol{a})|^2 \exp\left(\frac{E(\Delta\boldsymbol{\alpha},\boldsymbol{a})}{D}\right)d\boldsymbol{a}d\Delta\boldsymbol{\alpha}$$
$$\le C_7C_6|\Omega_{\rm TJ}|e^{-\frac{2\min\{3\gamma,\eta\}D}{C_4}t}, \tag{4.6}$$

hence the exponential decay estimate for ρ_1 is derived. Similarly, the estimates for $(\rho_1)_t$ and $\nabla^\Omega_{\Delta\boldsymbol{\alpha}}\rho_1$ can be deduced. □

Remark 4.1. Using the same argument as in the proof of Proposition 4.1, one can obtain similar long-time asymptotics for the probability density ρ_2. In this work, we are more interested in the analysis of the marginal probability density of the misorientations $\Delta\boldsymbol{\alpha}$, $\rho_1=\rho_1(\Delta\boldsymbol{\alpha},t)$ due to the relation to the GBCD statistical metric.

Next, we compare $\rho_{1,\infty}$ and the Boltzmann distribution of the misorientations $\Delta\boldsymbol{\alpha}$. We first derive the evolution equation for the marginal distribution ρ_1.

Proposition 4.2. *Let f be a solution of* (3.1)*, and let $\rho_1=\rho_1(\Delta\boldsymbol{\alpha},t)$ be a marginal distribution defined by* (4.1)*. Then, ρ_1 satisfies*

$$\frac{\partial\rho_1}{\partial t} = \frac{\beta^2_{\Delta\boldsymbol{\alpha}}}{2}\Delta^\Omega_{\Delta\boldsymbol{\alpha}}\rho_1 - \nabla^\Omega_{\Delta\boldsymbol{\alpha}}\cdot\left(\int_{\Omega_{\rm TJ}} (\boldsymbol{v}_{\Delta\boldsymbol{\alpha}}f)\,d\boldsymbol{a}\right), \quad \Delta\boldsymbol{\alpha}\in\Omega,\ t>0. \tag{4.7}$$

Proof. Integrate (3.1) in $\boldsymbol{a} \in \Omega_{\mathrm{TJ}}$, hence we obtain

$$\frac{\partial \rho_1}{\partial t} + \nabla^{\Omega}_{\Delta\boldsymbol{\alpha}} \cdot \left(\int_{\Omega_{\mathrm{TJ}}} (\boldsymbol{v}_{\Delta\boldsymbol{\alpha}} f)\, d\boldsymbol{a} \right) + \int_{\Omega_{\mathrm{TJ}}} \nabla_{\boldsymbol{a}} \cdot (\boldsymbol{v}_{\boldsymbol{a}} f)\, d\boldsymbol{a}$$
$$= \frac{\beta^2_{\Delta\boldsymbol{\alpha}}}{2} \Delta^{\Omega}_{\Delta\boldsymbol{\alpha}} \rho_1 + \frac{\beta^2_{\boldsymbol{a}}}{2} \int_{\Omega_{\mathrm{TJ}}} \Delta_{\boldsymbol{a}} f\, d\boldsymbol{a}. \tag{4.8}$$

Due to the boundary conditions of (3.1), it follows

$$\frac{\beta^2_{\boldsymbol{a}}}{2} \int_{\Omega_{\mathrm{TJ}}} \Delta_{\boldsymbol{a}} f\, d\boldsymbol{a} - \int_{\Omega_{\mathrm{TJ}}} \nabla_{\boldsymbol{a}} \cdot (\boldsymbol{v}_{\boldsymbol{a}} f)\, d\boldsymbol{a} = \int_{\partial\Omega_{\mathrm{TJ}}} \left(\frac{\beta^2_{\boldsymbol{a}}}{2} \nabla_{\boldsymbol{a}} f - \boldsymbol{v}_{\boldsymbol{a}} f \right) \cdot \boldsymbol{\nu}_{\boldsymbol{a}}\, dS_{\boldsymbol{a}} = 0 \tag{4.9}$$

for $\Delta\boldsymbol{\alpha} \in \Omega$, where $\boldsymbol{\nu}_{\boldsymbol{a}}$ is an outer unit normal on $\partial\Omega_{\mathrm{TJ}}$, and $dS_{\boldsymbol{a}}$ is a length element on $\partial\Omega_{\mathrm{TJ}}$. From (4.8) and (4.9), one can obtain (4.7). □

To proceed with the analysis of ρ_1, we first consider the Taylor expansion of the grain boundary energy E around arbitrarily selected point $\boldsymbol{a}_* \in \Omega_{\mathrm{TJ}}$, namely

$$E(\Delta\boldsymbol{\alpha}, \boldsymbol{a}) = \sum_{j=1}^{3} \sigma(\Delta^{(j)}\alpha) |\boldsymbol{a} - \boldsymbol{x}^{(j)}| = E_1(\Delta\boldsymbol{\alpha}) + E_2(\Delta\boldsymbol{\alpha}, \boldsymbol{a}), \tag{4.10}$$

where

$$E_1(\Delta\boldsymbol{\alpha}) = \sum_{j=1}^{3} \sigma(\Delta^{(j)}\alpha) |\boldsymbol{a}_* - \boldsymbol{x}^{(j)}|, \quad \text{and}$$
$$E_2(\Delta\boldsymbol{\alpha}, \boldsymbol{a}) = E(\Delta\boldsymbol{\alpha}, \boldsymbol{a}) - E_1(\Delta\boldsymbol{\alpha}). \tag{4.11}$$

Note that we formulated the grain boundary energy E in the form above (4.10) to investigate effect of the position of the triple junction $\boldsymbol{a} = \boldsymbol{a}_*$ on the distribution of the misorientations $\rho_1(\Delta\boldsymbol{\alpha}, t)$ and its steady-state distribution $\rho_{1,\infty}(\Delta\boldsymbol{\alpha})$.

Remark 4.2. From Proposition 4.1, marginal distribution ρ_1 may not converge to the Boltzmann distribution, in general. This is because

$$\rho_{1,\infty}(\Delta\boldsymbol{\alpha}) = \left(C_1 \int_{\Omega_{\mathrm{TJ}}} \exp\left(-\frac{E_2(\Delta\boldsymbol{\alpha}, \boldsymbol{a})}{D} \right) d\boldsymbol{a} \right) \exp\left(-\frac{E_1(\Delta\boldsymbol{\alpha})}{D} \right), \tag{4.12}$$

and the coefficient of $\exp(-E_1/D)$ generally depend on $\Delta\boldsymbol{\alpha}$.

Using (4.10), Eq. (4.7) becomes

$$\frac{\partial \rho_1}{\partial t} = \frac{\beta^2_{\Delta\boldsymbol{\alpha}}}{2} \Delta^{\Omega}_{\Delta\boldsymbol{\alpha}} \rho_1 - \nabla^{\Omega}_{\Delta\boldsymbol{\alpha}} \cdot \left((-3\gamma \nabla^{\Omega}_{\Delta\boldsymbol{\alpha}} E_1(\Delta\boldsymbol{\alpha})) \rho_1 \right)$$
$$+ 3\gamma \nabla^{\Omega}_{\Delta\boldsymbol{\alpha}} \cdot \left(\int_{\Omega_{\mathrm{TJ}}} \left((\nabla^{\Omega}_{\Delta\boldsymbol{\alpha}} E_2(\Delta\boldsymbol{\alpha}, \boldsymbol{a}))) f \right) d\boldsymbol{a} \right), \tag{4.13}$$

hence ρ_1 satisfies the Fokker–Planck type equation with an extra term.

Next, we explore the effects of the triple junction position, $\boldsymbol{a} = \boldsymbol{a}_*$ on (4.7).

Remark 4.3. In Refs. 3, 5, 6 and 7, Fokker–Planck equation was derived for the evolution of the GBCD using a novel implementation of the iterative scheme for the Fokker–Planck equation in terms of the system free energy and a Kantorovich–Rubinstein–Wasserstein metric. Equation for probability density of misorientations ρ_1, (4.7) or (4.13) is a Fokker–Planck type equation which also takes into account the effect of the mobility of the triple junctions.

Remark 4.4. Because of

$$\begin{aligned}\partial_{a_k}|\boldsymbol{a}-\boldsymbol{x}^{(j)}| &= \frac{a_k - x_k^{(j)}}{|\boldsymbol{a}-\boldsymbol{x}^{(j)}|},\\ \partial_{a_l}\partial_{a_k}|\boldsymbol{a}-\boldsymbol{x}^{(j)}| &= \frac{1}{|\boldsymbol{a}-\boldsymbol{x}^{(j)}|}\left(\delta_{kl} - \frac{a_k - x_k^{(j)}}{|\boldsymbol{a}-\boldsymbol{x}^{(j)}|}\frac{a_l - x_l^{(j)}}{|\boldsymbol{a}-\boldsymbol{x}^{(j)}|}\right),\end{aligned} \tag{4.14}$$

where δ_{kl} is the Kronecker delta, $\boldsymbol{a} = (a_1, a_2)$, and $\boldsymbol{x}^{(j)} = (x_1^{(j)}, x_2^{(j)})$, by the Taylor expansion for $|\boldsymbol{a}-\boldsymbol{x}^{(j)}|$ around $\boldsymbol{a}_*$ we obtain the following expansion for E_2;

$$\begin{aligned}E_2(\Delta\boldsymbol{\alpha}, \boldsymbol{a}) &= \sum_{j=1}^{3}\sigma(\Delta\alpha^{(j)})\left(|\boldsymbol{a}-\boldsymbol{x}^{(j)}| - |\boldsymbol{a}_*-\boldsymbol{x}^{(j)}|\right)\\ &= \sum_{j=1}^{3}\sigma(\Delta\alpha^{(j)})\left(\frac{(\boldsymbol{a}_*-\boldsymbol{x}^{(j)})}{|\boldsymbol{a}_*-\boldsymbol{x}^{(j)}|}\cdot(\boldsymbol{a}-\boldsymbol{a}_*)\right.\\ &\quad + \frac{1}{2|\boldsymbol{a}_*-\boldsymbol{x}^{(j)}|}\left(|\boldsymbol{a}-\boldsymbol{a}_*|^2 - \left(\frac{(\boldsymbol{a}_*-\boldsymbol{x}^{(j)})}{|\boldsymbol{a}_*-\boldsymbol{x}^{(j)}|}\cdot(\boldsymbol{a}-\boldsymbol{a}_*)\right)^2\right)\\ &\quad \left. + o(|\boldsymbol{a}-\boldsymbol{a}_*|^2)\right)\end{aligned} \tag{4.15}$$

as $\boldsymbol{a} \to \boldsymbol{a}_*$.

4.1. *The weighted Fermat–Torricelli point as a triple junction point*

Let $\boldsymbol{a}_*$ be the minimizer of $E(\Delta\boldsymbol{\alpha}, \boldsymbol{a})$, which is called the weighted Fermat–Torricelli point $\boldsymbol{a}_{\mathrm{wFT}}$, for fixed $\Delta\boldsymbol{\alpha} \in \Omega$ (cf. Ref. 13), that is

$$\sum_{j=1}^{3}\sigma(\Delta^{(j)}\alpha)|\boldsymbol{a}_{\mathrm{wFT}}-\boldsymbol{x}^{(j)}| = \inf_{\boldsymbol{a}\in\Omega_{\mathrm{TJ}}}\sum_{j=1}^{3}\sigma(\Delta^{(j)}\alpha)|\boldsymbol{a}-\boldsymbol{x}^{(j)}| = \inf_{\boldsymbol{a}\in\Omega_{\mathrm{TJ}}}E(\Delta\boldsymbol{\alpha}, \boldsymbol{a}). \tag{4.16}$$

Let $\psi^{(i)}$ be an angle formed by $\boldsymbol{a}-\boldsymbol{x}^{(i)}$ and $\boldsymbol{a}-\boldsymbol{x}^{(i+1)}$ at the triple junction $\boldsymbol{a}$. Now we give an equivalent condition that the triple junction coincides with $\boldsymbol{a}_{\mathrm{wFT}}$.

Proposition 4.3. *Assume that weighted Fermat–Torricelli point $\boldsymbol{a}_{\mathrm{wFT}}$ does not coincide with $\boldsymbol{x}^{(j)}$ for $j = 1, 2, 3$. Then, the triple junction coincides with $\boldsymbol{a}_{\mathrm{wFT}}$, if*

and only if,

$$1-\cos\psi^{(i)}=\frac{(\sigma(\Delta^{(i)}\alpha)+\sigma(\Delta^{(i+1)}\alpha))^2-\sigma(\Delta^{(i+2)}\alpha)^2}{2\sigma(\Delta^{(i)}\alpha)\sigma(\Delta^{(i+1)}\alpha)}, \tag{4.17}$$

for $i=1,2,3$.

Remark 4.5. A condition that for $k=1,2,3$,

$$\left|\sum_{\substack{1\le j\le 3,\\ j\neq k}}\sigma(\Delta^{(j)}\alpha)\frac{\boldsymbol{x}^{(j)}-\boldsymbol{x}^{(k)}}{|\boldsymbol{x}^{(j)}-\boldsymbol{x}^{(k)}|}\right|>\sigma(\Delta^{(k)}\alpha) \tag{4.18}$$

is equivalent to the condition that $\boldsymbol{a}_{\mathrm{wFT}}$ does not coincide with $\boldsymbol{x}^{(j)}$ for $j=1,2,3$ and

$$\begin{aligned}\boldsymbol{0}&=\nabla_{\boldsymbol{a}}E(\Delta\boldsymbol{\alpha},\boldsymbol{a}_{\mathrm{wFT}})=\sum_{j=1}^{3}\sigma(\Delta^{(j)}\alpha)\boldsymbol{e}^{(j)},\\ \boldsymbol{e}^{(j)}&:=\frac{\boldsymbol{a}_{\mathrm{wFT}}-\boldsymbol{x}^{(j)}}{|\boldsymbol{a}_{\mathrm{wFT}}-\boldsymbol{x}^{(j)}|}\end{aligned} \tag{4.19}$$

holds (see Ref. 13, Theorem 18.37).

Because, by (4.18),

$$\sigma(\Delta^{(k)}\alpha)<\left|\sigma(\Delta^{(i)}\alpha)\frac{\boldsymbol{x}^{(i)}-\boldsymbol{x}^{(k)}}{|\boldsymbol{x}^{(i)}-\boldsymbol{x}^{(k)}|}+\sigma(\Delta^{(j)}\alpha)\frac{\boldsymbol{x}^{(j)}-\boldsymbol{x}^{(k)}}{|\boldsymbol{x}^{(j)}-\boldsymbol{x}^{(k)}|}\right|$$

for different $1\le i,j,k\le 3$, one can obtain the following condition,

$$\sigma(\Delta^{(k)}\alpha)<\sigma(\Delta^{(i)}\alpha)+\sigma(\Delta^{(j)}\alpha). \tag{4.20}$$

Proof of Proposition 4.3. When $\boldsymbol{a}_{\mathrm{wFT}}$ does not coincide with $\boldsymbol{x}^{(j)}$ for $j=1,2,3$, the weighted Fermat–Torricelli point $\boldsymbol{a}_{\mathrm{wFT}}$ satisfies (4.19). Taking the inner product of (4.19) with $\boldsymbol{e}^{(k)}$ for $k=1,2,3$, we obtain

$$\begin{cases}\sigma(\Delta^{(2)}\alpha)(\boldsymbol{e}^{(1)},\boldsymbol{e}^{(2)})+\sigma(\Delta^{(3)}\alpha)(\boldsymbol{e}^{(3)},\boldsymbol{e}^{(1)})=-\sigma(\Delta^{(1)}\alpha),\\ \sigma(\Delta^{(1)}\alpha)(\boldsymbol{e}^{(1)},\boldsymbol{e}^{(2)})+\sigma(\Delta^{(3)}\alpha)(\boldsymbol{e}^{(2)},\boldsymbol{e}^{(3)})=-\sigma(\Delta^{(2)}\alpha),\\ \sigma(\Delta^{(2)}\alpha)(\boldsymbol{e}^{(2)},\boldsymbol{e}^{(3)})+\sigma(\Delta^{(1)}\alpha)(\boldsymbol{e}^{(3)},\boldsymbol{e}^{(1)})=-\sigma(\Delta^{(3)}\alpha).\end{cases} \tag{4.21}$$

Next, we can solve $(\boldsymbol{e}^{(k)},\boldsymbol{e}^{(l)})$ from (4.21) and, thus, obtain

$$\begin{aligned}(\boldsymbol{e}^{(1)},\boldsymbol{e}^{(2)})&=\frac{-(\sigma(\Delta^{(1)}\alpha))^2-(\sigma(\Delta^{(2)}\alpha))^2+(\sigma(\Delta^{(3)}\alpha))^2}{2\sigma(\Delta^{(1)}\alpha)\sigma(\Delta^{(2)}\alpha)},\\ (\boldsymbol{e}^{(2)},\boldsymbol{e}^{(3)})&=\frac{-(\sigma(\Delta^{(2)}\alpha))^2-(\sigma(\Delta^{(3)}\alpha))^2+(\sigma(\Delta^{(1)}\alpha))^2}{2\sigma(\Delta^{(2)}\alpha)\sigma(\Delta^{(3)}\alpha)},\\ (\boldsymbol{e}^{(3)},\boldsymbol{e}^{(1)})&=\frac{-(\sigma(\Delta^{(3)}\alpha))^2-(\sigma(\Delta^{(1)}\alpha))^2+(\sigma(\Delta^{(2)}\alpha))^2}{2\sigma(\Delta^{(3)}\alpha)\sigma(\Delta^{(1)}\alpha)}.\end{aligned} \tag{4.22}$$

Note that $(\boldsymbol{e}^{(k)}, \boldsymbol{e}^{(l)})$ is the cosine of the angle at $\boldsymbol{a}_{\mathrm{wFT}}$ formed by $\boldsymbol{e}^{(k)}$ and $\boldsymbol{e}^{(l)}$. Thus, we have

$$\begin{aligned}
\cos\psi^{(1)} &= \frac{-(\sigma(\Delta^{(1)}\alpha))^2 - (\sigma(\Delta^{(2)}\alpha))^2 + (\sigma(\Delta^{(3)}\alpha))^2}{2\sigma(\Delta^{(1)}\alpha)\sigma(\Delta^{(2)}\alpha)},\\
\cos\psi^{(2)} &= \frac{-(\sigma(\Delta^{(2)}\alpha))^2 - (\sigma(\Delta^{(3)}\alpha))^2 + (\sigma(\Delta^{(1)}\alpha))^2}{2\sigma(\Delta^{(2)}\alpha)\sigma(\Delta^{(3)}\alpha)},\\
\cos\psi^{(3)} &= \frac{-(\sigma(\Delta^{(3)}\alpha))^2 - (\sigma(\Delta^{(1)}\alpha))^2 + (\sigma(\Delta^{(2)}\alpha))^2}{2\sigma(\Delta^{(3)}\alpha)\sigma(\Delta^{(1)}\alpha)},
\end{aligned} \tag{4.23}$$

hence we arrive at (4.17) by direct calculation of $1 - \cos\psi^{(i)}$.

Conversely, when (4.17) holds for the triple junction $\boldsymbol{a}$, then the triple junction $\boldsymbol{a}$ satisfies the same conditions as $\boldsymbol{a}_{\mathrm{wFT}}$ in (4.19) and in (4.21). Since the weighted Fermat–Torricelli point is unique (see Ref. 13, Theorem 18.37), $\boldsymbol{a}_{\mathrm{wFT}}$ coincides with the triple junction $\boldsymbol{a}$. □

Remark 4.6. The relation (4.17) is a force balance condition at the triple junction, the generalized Herring condition. When $\sigma \equiv 1$, then from (4.17) we have $\cos\psi^{(i)} = -1/2$, hence three angles at the triple junction are the same, $\frac{2\pi}{3}$.

Next, we study the behavior of the reminder term E_2 when $\boldsymbol{a}_* = \boldsymbol{a}_{\mathrm{wFT}}$. Thanks to $\nabla_{\boldsymbol{a}} E(\Delta\boldsymbol{\alpha}, \boldsymbol{a}_*) = \boldsymbol{0}$, one can obtain the following result.

Proposition 4.4. *Assume that weighted Fermat–Torricelli point $\boldsymbol{a}_{\mathrm{wFT}}$ does not coincide with $\boldsymbol{x}^{(j)}$ for $j = 1, 2, 3$. Let $\boldsymbol{a}_* = \boldsymbol{a}_{\mathrm{wFT}}$. Then,*

$$\begin{aligned}
E_2(\Delta\boldsymbol{\alpha}, \boldsymbol{a}) = \sum_{j=1}^{3} \sigma(\Delta^{(j)}\alpha)\Bigg(&\frac{1}{2|\boldsymbol{a}_* - \boldsymbol{x}^{(j)}|}\left(|\boldsymbol{a} - \boldsymbol{a}_*|^2 - \left(\frac{(\boldsymbol{a}_* - \boldsymbol{x}^{(j)})}{|\boldsymbol{a}_* - \boldsymbol{x}^{(j)}|}\cdot(\boldsymbol{a} - \boldsymbol{a}_*)\right)^2\right)\\
&+ o(|\boldsymbol{a} - \boldsymbol{a}_*|^2)\Bigg)
\end{aligned} \tag{4.24}$$

as $\boldsymbol{a} \to \boldsymbol{a}_*$.

Proof. Since $\nabla_{\boldsymbol{a}} E(\Delta\boldsymbol{\alpha}, \boldsymbol{a}_*) = \boldsymbol{0}$, by (4.19) we have that

$$\sum_{j=1}^{3} \sigma(\Delta\alpha^{(j)}) \frac{(\boldsymbol{a}_* - \boldsymbol{x}^{(j)})}{|\boldsymbol{a}_* - \boldsymbol{x}^{(j)}|} = \boldsymbol{0}.$$

Using this in (4.15), we obtain (4.24). □

The above Proposition 4.4 is a reason of why we choose $\boldsymbol{a}_{\mathrm{wFT}}$ as $\boldsymbol{a}_*$, namely, we can show that E_2 is asymptotically of order $|\boldsymbol{a} - \boldsymbol{a}_*|^2$ as $\boldsymbol{a} \to \boldsymbol{a}_*$.

4.2. *The circumcenter as a triple junction point*

Next, we introduce the circumcenter $\boldsymbol{a}_{\rm cc}$ of $\boldsymbol{x}^{(j)}$. The circumcircle of $\boldsymbol{x}^{(j)}$ is the unique circle that passes through all $\boldsymbol{x}^{(j)}$, and the circumcenter $\boldsymbol{a}_{\rm cc}$ of $\boldsymbol{x}^{(j)}$ is the center of the circumcircle, namely

$$|\boldsymbol{a}_{\rm cc} - \boldsymbol{x}^{(1)}| = |\boldsymbol{a}_{\rm cc} - \boldsymbol{x}^{(2)}| = |\boldsymbol{a}_{\rm cc} - \boldsymbol{x}^{(3)}|. \tag{4.25}$$

If a triple junction $\boldsymbol{a}$ coincides with the circumcenter then, Boltzmann distribution $\exp(-\frac{E_1}{D})$ becomes Boltzmann distribution for a grain boundary energy density $\sigma(\Delta^{(j)}\alpha)$ (instead of Boltzmann distribution for the grain boundary energy E), namely

$$E_1(\Delta\boldsymbol{\alpha}) = |\boldsymbol{a}_{\rm cc} - \boldsymbol{x}^{(1)}| \sum_{j=1}^{3} \sigma(\Delta^{(j)}\alpha). \tag{4.26}$$

This is reminiscent of the result for the steady-state GBCD which is given by the Boltzmann distribution for the grain boundary energy density, see for instance Refs. 3, 5, 6 and 7. When $\boldsymbol{a}_*$ coincides with $\boldsymbol{a}_{\rm cc}$, from (4.12) and (4.26), $\rho_{1,\infty}$ is similar to $\exp(-\frac{|\boldsymbol{a}_{\rm cc}-\boldsymbol{x}^{(1)}|}{D} \sum_{j=1}^{3} \sigma(\Delta^{(j)}\alpha))$.

We now give a relation between the angle at the circumcenter point and the point $\boldsymbol{x}^{(j)}$.

Proposition 4.5. *If the triple junction coincides with the circumcenter* $\boldsymbol{a}_{\rm cc}$*, then*

$$\frac{1-\cos\psi^{(1)}}{|\boldsymbol{x}^{(1)} - \boldsymbol{x}^{(2)}|^2} = \frac{1-\cos\psi^{(2)}}{|\boldsymbol{x}^{(2)} - \boldsymbol{x}^{(3)}|^2} = \frac{1-\cos\psi^{(3)}}{|\boldsymbol{x}^{(3)} - \boldsymbol{x}^{(1)}|^2}. \tag{4.27}$$

Proof. By the cosine formula, for $i = 1, 2, 3$,

$$\begin{aligned} |\boldsymbol{x}^{(i)} - \boldsymbol{x}^{(i+1)}|^2 &= |\boldsymbol{a}_{\rm cc} - \boldsymbol{x}^{(i)}|^2 + |\boldsymbol{a}_{\rm cc} - \boldsymbol{x}^{(i+1)}|^2 \\ &\quad - 2|\boldsymbol{a}_{\rm cc} - \boldsymbol{x}^{(i)}||\boldsymbol{a}_{\rm cc} - \boldsymbol{x}^{(i+1)}|(\boldsymbol{e}^{(i)}, \boldsymbol{e}^{(i+1)}) \\ &= 2R^2(1-\cos\psi^{(i)}), \end{aligned}$$

where $R = |\boldsymbol{a}_{\rm cc} - \boldsymbol{x}^{(1)}| = |\boldsymbol{a}_{\rm cc} - \boldsymbol{x}^{(2)}| = |\boldsymbol{a}_{\rm cc} - \boldsymbol{x}^{(3)}|$. Thus,

$$\frac{1}{2R^2} = \frac{1-\cos\psi^{(1)}}{|\boldsymbol{x}^{(1)} - \boldsymbol{x}^{(2)}|^2} = \frac{1-\cos\psi^{(2)}}{|\boldsymbol{x}^{(2)} - \boldsymbol{x}^{(3)}|^2} = \frac{1-\cos\psi^{(3)}}{|\boldsymbol{x}^{(3)} - \boldsymbol{x}^{(1)}|^2},$$

hence (4.27) holds. □

Next we look at a necessary condition for $\boldsymbol{a}_{\rm wFT} = \boldsymbol{a}_{\rm cc}$. By combining the relations (4.17) and (4.27), we have the following corollary.

Corollary 4.1. *Assume that weighted Fermat–Torricelli point* $\boldsymbol{a}_{\rm wFT}$ *does not coincide with* $\boldsymbol{x}^{(j)}$ *for* $j = 1, 2, 3$*. If the triple junction,* $\boldsymbol{a}_{\rm wFT}$*, and circumcenter* $\boldsymbol{a}_{\rm cc}$ *are*

all the same, then,

$$\frac{(\sigma(\Delta^{(1)}\alpha)+\sigma(\Delta^{(2)}\alpha))^2-\sigma(\Delta^{(3)}\alpha)^2}{2\sigma(\Delta^{(1)}\alpha)\sigma(\Delta^{(2)}\alpha)|\boldsymbol{x}^{(1)}-\boldsymbol{x}^{(2)}|^2}=\frac{(\sigma(\Delta^{(2)}\alpha)+\sigma(\Delta^{(3)}\alpha))^2-\sigma(\Delta^{(1)}\alpha)^2}{2\sigma(\Delta^{(2)}\alpha)\sigma(\Delta^{(3)}\alpha)|\boldsymbol{x}^{(2)}-\boldsymbol{x}^{(3)}|^2}$$
$$=\frac{(\sigma(\Delta^{(3)}\alpha)+\sigma(\Delta^{(1)}\alpha))^2-\sigma(\Delta^{(2)}\alpha)^2}{2\sigma(\Delta^{(3)}\alpha)\sigma(\Delta^{(1)}\alpha)|\boldsymbol{x}^{(3)}-\boldsymbol{x}^{(1)}|^2}. \tag{4.28}$$

Remark 4.7. When $\sigma\equiv 1$, then the relation (4.28) gives

$$|\boldsymbol{x}^{(1)}-\boldsymbol{x}^{(2)}|=|\boldsymbol{x}^{(2)}-\boldsymbol{x}^{(3)}|=|\boldsymbol{x}^{(3)}-\boldsymbol{x}^{(1)}|,$$

hence $\boldsymbol{x}^{(1)}$, $\boldsymbol{x}^{(2)}$, $\boldsymbol{x}^{(3)}$ are vertices of some equilateral triangle. Thus, (4.28) is a more general "geometric" condition on $\boldsymbol{x}^{(j)}$ and the grain boundary energy density $\sigma(\Delta\boldsymbol{\alpha})$ to observe Boltzmann distribution for a grain boundary energy density as a steady-state distribution for $\rho_1(\Delta\boldsymbol{\alpha},t)$.

5. Numerical Experiments

Here, we present several numerical experiments to illustrate consistency of the proposed stochastic model (2.15) with a grain growth model (2.2) applied to a grain boundary network that undergoes critical/disappearance events, e.g. grain disappearance, facet/grain boundary disappearance, facet interchange, splitting of unstable junctions. We define the total grain boundary energy of the network, like

$$E(t)=\sum_j \sigma(\Delta^{(j)}\alpha)|\Gamma_t^{(j)}|, \tag{5.1}$$

where $\Delta^{(j)}\alpha$ is a misorientation, a difference between the lattice orientation of the two neighboring grains which form the grain boundary $\Gamma_t^{(j)}$. Then, the energetic variational principle implies

$$\begin{cases} v_n^{(j)}=\mu\sigma(\Delta^{(j)}\alpha)\kappa^{(j)}, \quad \text{on } \Gamma_t^{(j)},\ t>0,\\ \dfrac{d\alpha^{(k)}}{dt}=-\gamma\dfrac{\delta E}{\delta\alpha^{(k)}},\\ \dfrac{d\boldsymbol{a}^{(l)}}{dt}=\eta\displaystyle\sum_{\boldsymbol{a}^{(l)}\in\Gamma_t^{(j)}}\left(\sigma(\Delta^{(j)}\alpha)\frac{\boldsymbol{b}^{(j)}}{|\boldsymbol{b}^{(j)}|}\right), \quad t>0. \end{cases} \tag{5.2}$$

First, we will test "generalized" Herring condition (4.17), as well as relations (4.27) and (4.28) for the grain boundary network (5.2). Next, in our numerics, using grain boundary character distribution (GBCD) statistics (see for example Refs. 3, 5, 6 and 7), we will illustrate that the grain growth system (5.2) exhibits some fluctuation–dissipation principles (see Sec. 2.2).

Therefore, to verify first "generalized" Herring condition (4.17), we define ratio R_1,

$$R_1 := \frac{(\sigma(\Delta^{(i)}\alpha) + \sigma(\Delta^{(i+1)}\alpha))^2 - \sigma(\Delta^{(i+2)}\alpha)^2}{2(1-\cos\psi^{(i)})\sigma(\Delta^{(i)}\alpha)\sigma(\Delta^{(i+1)}\alpha)}, \quad i = 1, 2, 3, \ldots. \tag{5.3}$$

To verify relations (4.27) and (4.28), we define ratio R_2 and R_3 respectively for each triple junction $\boldsymbol{a}$,

$$R_2 := \frac{|\boldsymbol{x}^{(3)} - \boldsymbol{x}^{(1)}|^2\sqrt{(1-\cos\psi^{(1)})(1-\cos\psi^{(2)})}}{(1-\cos\psi^{(3)})|\boldsymbol{x}^{(1)} - \boldsymbol{x}^{(2)}||\boldsymbol{x}^{(2)} - \boldsymbol{x}^{(3)}|}, \tag{5.4}$$

and

$$R_3 := \frac{\sqrt{\mathcal{R}_1 \cdot \mathcal{R}_2}}{\mathcal{R}_3}, \tag{5.5}$$

where $\mathcal{R}_i := \frac{(\sigma(\Delta^{(i)}\alpha)+\sigma(\Delta^{(i+1)}\alpha))^2-\sigma(\Delta^{(i+2)}\alpha)^2}{2|\boldsymbol{x}^{(i)}-\boldsymbol{x}^{(i+1)}|^2\sigma(\Delta^{(i)}\alpha)\sigma(\Delta^{(i+1)}\alpha)}$ and $\boldsymbol{x}^{(i)} \neq \boldsymbol{a}$ are any node along grain boundary with triple junction $\boldsymbol{a}$. Note that formulas for R_2 and R_3 (5.4)–(5.5) require selection of the node x_i along the grain boundary different from the triple junction $\boldsymbol{a}$, see for example Figs. 1 and 2. Note also that for $j = 1, 2, 3$, R_j is a dimensionless quantity with respect to the length of grain boundaries. If the formula (4.17), (4.27), or (4.28) holds, then $R_j = 1$ ($j = 1, 2, 3$), respectively. Moreover, since (4.17), (4.27), and (4.28) are local relations (*and not the property of the network*), we don't expect for these relations to hold exactly, and hence, in our numerical experiments we compute probability densities for R_1, as well as for R_2 and R_3 (using two choices of the node x_i to compute R_2 and R_3). In Figs. 5,

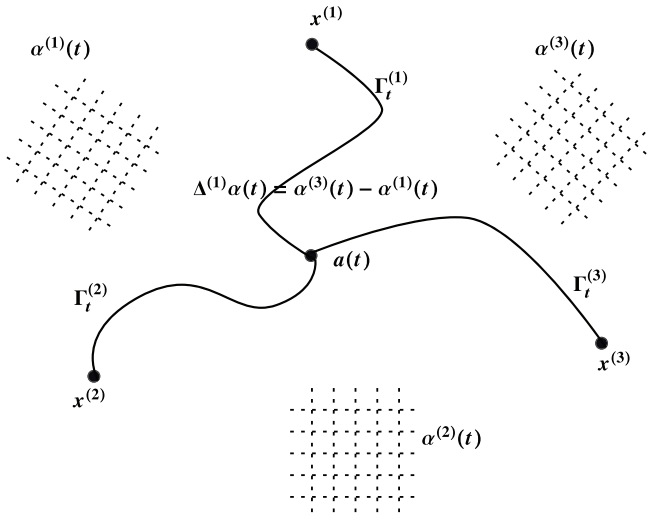

Fig. 1. Grain boundaries/curves $\Gamma_t^{(j)}$ that meet at a triple junction $\boldsymbol{a}(t)$. Lattice orientations are angles (scalars) $\alpha^{(j)}(t)$. Misorientation $\Delta^{(j)}\alpha(t)$ of $\Gamma_t^{(j)}$ is the difference between two lattice orientations of grains that share grain boundary $\Gamma_t^{(j)}$.

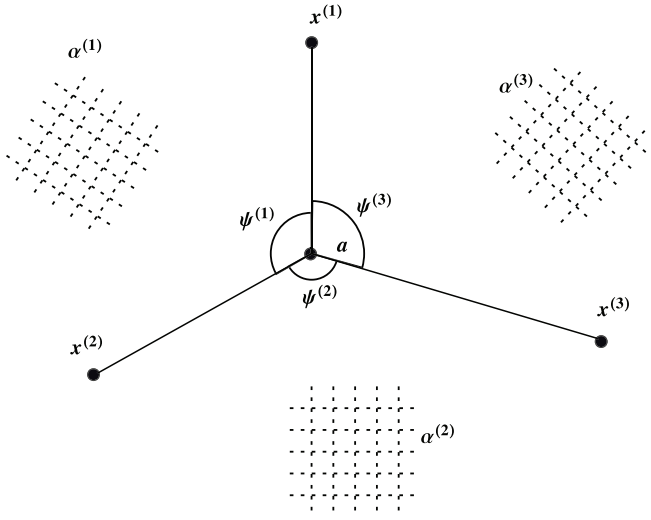

Fig. 2. The angles ψ_1, ψ_2, ψ_3 are defined as the above figure.

6, 8, 10, 11 (left plot) and 13 (left and middle plots) we selected x_i to be a mesh node on the grain boundary which is the closest to the triple junction $\boldsymbol{a}$ (note, we discretize each grain boundary using linear line segments, hence, end points of these line segments form mesh nodes on each grain boundary). As a second choice for the node x_i, see Fig. 7, we selected x_i to be the other end point of the grain boundary/the "other triple junction" (different from the triple junction of $\boldsymbol{a}$) of the considered grain boundary that shares $\boldsymbol{a}$. As our results show, choice of x_i affects the distributions for R_2 and R_3. However, the choice of x_i does not affect consistency property reflected by distributions for R_2 and R_3 between developed stochastic model (2.15) and the simulated grain growth system (5.2), see Figs. 5, 6, 8, 10, 11 (left plot), 13 (left and middle plots) and Fig. 7.

Further, we will investigate the distribution of the grain boundary character distribution (GBCD) $\rho(\Delta^{(j)}\alpha)$ at T_∞ (T_∞ is defined below), and we will use GBCD to illustrate that the grain growth system (5.2) exhibits some fluctuation–dissipation principles (see Sec. 2.2). The GBCD (in our context) is an empirical statistical measure of the relative length (in 2D) of the grain boundary interface with a given lattice misorientation,

$$\rho(\Delta^{(j)}\alpha, t) = \text{relative length of interface of lattice misorientation } \Delta^{(j)}\alpha \text{ at time } t,$$
$$\text{normalized so that } \int_{\Omega_{\Delta^{(j)}\alpha}} \rho d\Delta^{(j)}\alpha = 1, \tag{5.6}$$

where we consider $\Omega_{\Delta^{(j)}\alpha} = [-\frac{\pi}{4}, \frac{\pi}{4}]$ in the numerical experiments below (for planar grain boundary network, it is reasonable to consider such range for the misorientations). For more details, see for example Ref. 5. In all our tests below, we compare

GBCD at T_∞ to the stationary solution of the Fokker–Planck equation, the Boltzmann distribution for the grain boundary energy density $\sigma(\Delta^{(j)}\alpha)$,

$$\rho_D(\Delta^{(j)}\alpha) = \frac{1}{Z_D} e^{-\frac{\sigma(\Delta^{(j)}\alpha)}{D}},$$

with partition function, i.e. normalization factor (5.7)

$$Z_D = \int_{\Omega_{\Delta^{(j)}\alpha}} e^{-\frac{\sigma(\Delta^{(j)}\alpha)}{D}} d\Delta^{(j)}\alpha,$$

see Refs. 3, 5, 6 and 7 and Sec. 4. We employ Kullback–Leibler relative entropy test to obtain a unique "temperature-like" parameter D and to construct the corresponding Boltzmann distribution for the GBCD at T_∞ as it was originally done in Refs. 3, 5, 6 and 7. Kullback–Leibler (KL) relative entropy test[3, 5–7] is based on the idea that if we know that the GBCD $\rho(\Delta^{(j)}\alpha, t)$ evolves according to the Fokker–Planck equation, then it must converge exponentially fast to $\rho_D(\Delta^{(j)}\alpha)$ in KL relative entropy as $t \to \infty$. Note that the GBCD is a primary candidate to characterize texture of the grain boundary network, and is inversely related to the grain boundary energy density as discovered in experiments and simulations. The reader can consult for example Refs. 3, 5, 6 and 7 for more details about GBCD and the theory of the GBCD. In the numerical experiments in this paper, we consider the grain boundary energy density as plotted in Fig. 3 and given below:

$$\sigma(\Delta^{(j)}\alpha) = 1 + 0.25\sin^2(2\Delta^{(j)}\alpha).$$

Our simulation of 2D grain boundary network[20] is a further extension of the algorithm based on sharp interface approach[3, 6] (note, that in Refs. 3 and 6, only Herring conditions at triple junctions were considered, i.e. $\eta \to \infty$, and dynamic orientations/misorientations ("rotation of grains") was absent, i.e. $\gamma = 0$). We recall that in the numerical scheme we work with a variational principle. The cornerstone of the algorithm, which assures its stability, is the discrete dissipation inequality

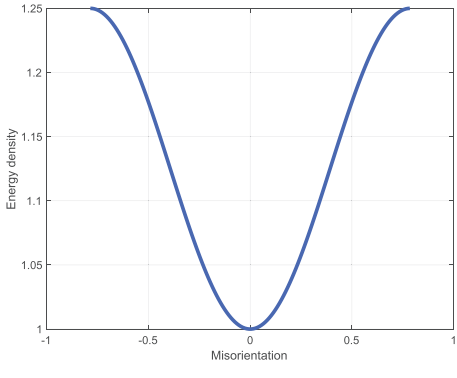

Fig. 3. Grain boundary energy density function $\sigma(\Delta\alpha)$.

for the total grain boundary energy that holds when either the discrete Herring boundary condition ($\eta \to \infty$) or discrete "dynamic boundary condition" (finite mobility η of the triple junctions, third equation of (5.2)) is satisfied at the triple junctions. We also recall that in the numerical algorithm we impose Mullins theory (first equation of (5.2)) as the local evolution law for the grain boundaries (and the relaxation time scale μ is kept finite). For more details about computational model based on Mullins equations (curvature driven growth), the reader can consult for example Refs. 3, 6 and 20. In addition, in our final test Fig. 13, we also compare results of "curvature model" (μ is finite) (5.2) with the results of "vertex model" ($\mu \to \infty$), grain boundaries are straight lines, and hence, only second and third evolution equations of (5.2) are considered for the vertex model, namely model (2.7) which is applied to the grain boundary network is studied.

In all the numerical tests below we initialized our system with $\mathcal{N}$ grains cells/grains with normally distributed misorientation angles at initial time $t = 0$. We also assume that the final time of the simulations T_∞ is the time when approximately 80% of grains disappeared from the system. The final time is selected based on the system with no dynamic misorientations ($\gamma = 0$) and with Herring condition at the triple junctions ($\eta \to \infty$) and, it is selected to ensure that statistically significant number of grains still remain in the system and the system reached its statistical stead-state. Therefore, all the numerical results which are presented below are for the grain boundary system that undergoes critical/disappearance events. We also denote by T_0 the initial time (before first time step) and by T_1 we denote a time after a first time step.

First, we consider grain growth model with curvature (5.2) and we study three systems with $\mathcal{N} = 10,000$ initial grains, the first system has $\gamma = 10$ and $\eta = 100$, the second system has $\gamma = 100$ and $\eta = 1000$, and the third system has $\gamma = 1000$ and $\eta \to \infty$ (Herring condition). We check "generalized" Herring condition formula (4.17) by computing probability density for ratio R_1, (5.3) and by computing time evolution of frequency of dihedral angles that satisfy ratio R_1 with 0.01 accuracy. The results for R_1 are plotted on Fig. 4. We observe that all three distributions of R_1 (left and middle plots) for all three grain growth systems have peak at 1 which is consistent with the "generalized" Herring condition formula (4.17). In addition, larger values of γ and of η provide a higher accuracy for ratio R_1 and, in addition, produce a higher peak of the distribution at 1. The distribution of R_1 for system with $\gamma = 1000$ and $\eta \to \infty$ (Herring condition) looks like a delta function positioned at 1 which is again consistent with results for the developed stochastic model Secs. 2.2–4. Next, we check relations (4.27) and (4.28) for the same three grain growth systems (5.2) by computing probability densities for ratio R_2 and R_3, (5.4) and (5.5). The results are presented in Figs. 5–8. Again, we observe that the peaks of the distributions for R_2 and R_3 for all three systems are near 1. Moreover, the agreement between distributions R_2 and R_3 is better for grain growth systems with larger values of γ and η (for $\gamma = 1000$ and $\eta \to \infty$, the plots for R_2 and R_3 are almost indistinguishable, see Figs. 6 (left plot) and 7 (right plot)), which is again

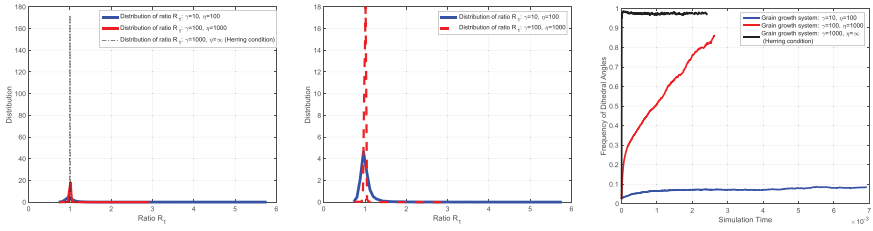

(a) (b) (c)

Fig. 4. (Color online) Grain growth system (5.2) with finite μ (with curvature), one run of 2D trial with 10,000 initial grains: (a) Left plot, distribution of ratio R_1 (5.3) for grain growth systems with mobility of triple junctions $\eta = 100$ and the misorientation parameter $\gamma = 10$ (solid blue), with mobility of triple junctions $\eta = 1000$ and the misorientation parameter $\gamma = 100$ (solid red) and with mobility of triple junctions $\eta \to \infty$ (Herring condition) and the misorientation parameter $\gamma = 1000$ (dashed point black). (b) Middle plot, comparison of the two distributions of ratio R_1 (5.3) for grain growth systems with mobility of triple junctions $\eta = 100$ and the misorientation parameter $\gamma = 10$ (solid blue) and with mobility of triple junctions $\eta = 1000$ and the misorientation parameter $\gamma = 100$ (dashed red). The distributions are plotted at T_∞. (c) Right plot, time evolution of frequency of dihedral angles that satisfy ratio R_1 with 0.01 accuracy for grain growth systems with mobility of triple junctions $\eta = 100$ and the misorientation parameter $\gamma = 10$ (solid blue), with mobility of triple junctions $\eta = 1000$ and the misorientation parameter $\gamma = 100$ (solid red) and with mobility of triple junctions $\eta \to \infty$ (Herring condition) and the misorientation parameter $\gamma = 1000$ (solid black).

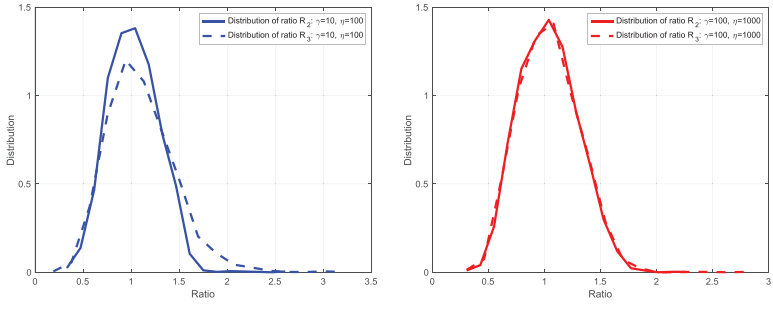

(a) (b)

Fig. 5. (Color online) Grain growth system (5.2) with finite μ (with curvature), one run of 2D trial with 10,000 initial grains: (a) Left plot, comparison of distributions of ratio R_2 (5.4) (solid blue) and R_3 (5.5) (dashed blue) for grain growth system with mobility of triple junctions $\eta = 100$ and the misorientation parameter $\gamma = 10$. (b) Right plot, comparison of distributions of ratio R_2 (5.4) (solid red) and R_3 (5.5) (dashed red) for grain growth system with mobility of triple junctions $\eta = 1000$ and the misorientation parameter $\gamma = 100$. The closest mesh node of the grain boundary to the triple junction $\boldsymbol{a}$ is used as x_i. The distributions are plotted at T_∞.

consistent with a developed theory, see Sec. 4. In addition, on Fig. 8, we illustrate how distribution for ratio R_3 evolves with time for grain growth system with $\gamma = 10$ and $\eta = 100$, Fig. 8 (left plot) and with $\gamma = 1000$ and $\eta \to \infty$ (Herring condition) Fig. 8 (right plot). The results illustrate that the distributions are "defined" by the grain growth evolution equations and not by the initial distribution. Finally, in the

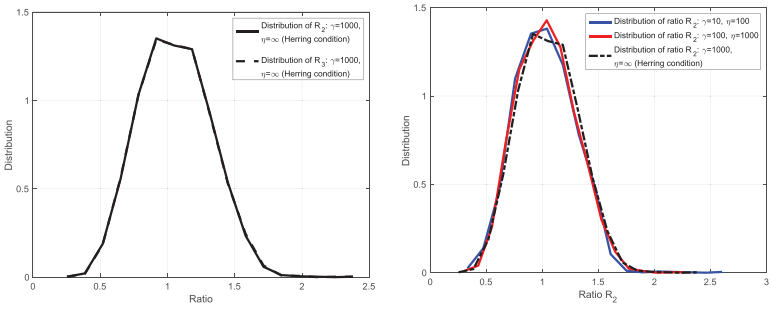

(a) (b)

Fig. 6. (Color online) Grain growth system (5.2) with finite μ (with curvature), one run of 2D trial with 10,000 initial grains: (a) Left plot, comparison of distributions of ratio R_2 (5.4) (solid black) and R_3 (5.5) (dashed black) for grain growth system with mobility of triple junctions $\eta \to \infty$ (Herring condition) and the misorientation parameter $\gamma = 1000$. (b) Right plot, comparison of distributions of ratio R_2 (5.4) for grain growth systems with mobility of triple junctions $\eta = 100$ and the misorientation parameter $\gamma = 10$ (solid blue), with mobility of triple junctions $\eta = 1000$ and the misorientation parameter $\gamma = 100$ (solid red), and with mobility of triple junctions $\eta \to \infty$ (Herring condition) and the misorientation parameter $\gamma = 1000$ (dashed point black). The closest mesh node of the grain boundary to the triple junction $\boldsymbol{a}$ is used as x_i. The distributions are plotted at T_∞.

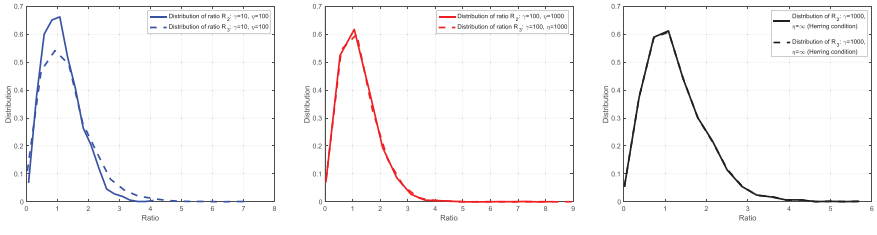

(a) (b) (c)

Fig. 7. (Color online) Grain growth system (5.2) with finite μ (with curvature), one run of 2D trial with 10,000 initial grains: (a) Left plot, comparison of distributions of ratio R_2 (5.4) (solid blue) and R_3 (5.5) (dashed blue) for grain growth system with mobility of triple junctions $\eta = 100$ and the misorientation parameter $\gamma = 10$. (b) Middle plot, comparison of distributions of ratio R_2 (5.4) (solid red) and R_3 (5.5) (dashed red) for grain growth systems with mobility of triple junctions $\eta = 1000$ and the misorientation parameter $\gamma = 100$. (c) Right plot, comparison of distributions of ratio R_2 (5.4) (solid black) and R_3 (5.5) (dashed black) for grain growth system with mobility of triple junctions $\eta \to \infty$ and the misorientation parameter $\gamma = 1000$. The other triple junction (different from **a**) of the given grain boundary is used as x_i here. The distributions are plotted at T_∞.

last test for the considered three grain growth systems, we compute GBCD statistics at time T_∞. First, we observe that the GBCD at T_∞ is well-approximated by the Boltzmann distribution for the grain boundary energy density see Fig. 9, which is consistent with the theory developed in the work[3, 5–7] and is consistent with the stochastic model and theory developed in this work, Secs. 2.2–4. Furthermore, as concluded from our numerical results Fig. 9, grain growth systems with larger

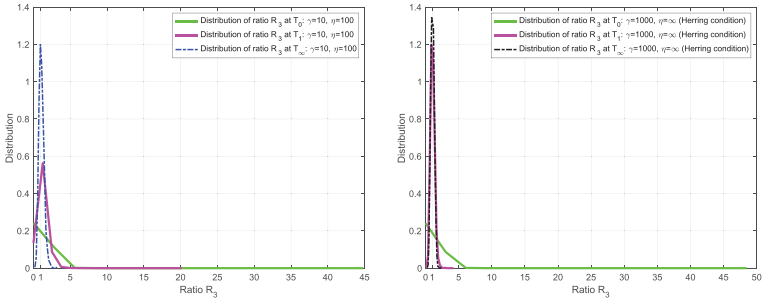

(a) (b)

Fig. 8. (Color online) Grain growth system (5.2) with finite μ (with curvature), one run of 2D trial with 10,000 initial grains: (a) Left plot, distributions of ratio R_3 (5.5) at initial time T_0 (solid green), at a time T_1 after a first time step (solid magenta) and at a final time T_∞ (dashed point blue) for grain growth system with mobility of triple junctions $\eta = 100$ and the misorientation parameter $\gamma = 10$. (b) Right plot, distributions of ratio R_3 (5.5) at initial time T_0 (solid green), at a time T_1 after a first time step (solid magenta) and at a final time T_∞ (dashed point black) for grain growth system with mobility of triple junctions $\eta \to \infty$ (Herring condition) and the misorientation parameter $\gamma = 1000$. The closest mesh node of the grain boundary to the triple junction $\boldsymbol{a}$ is used as x_i.

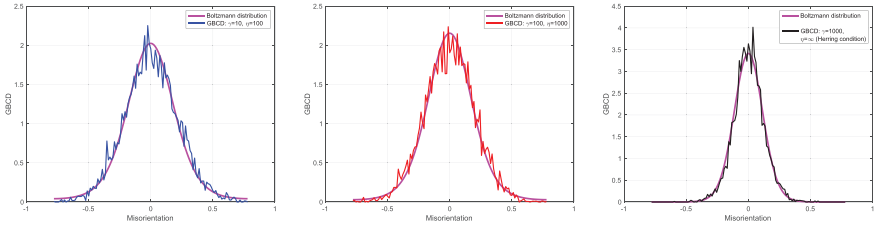

(a) (b) (c)

Fig. 9. (Color online) Grain growth system (5.2) with finite μ (with curvature), one run of 2D trial with 10,000 initial grains: (a) Left plot, GBCD (blue curve) at T_∞ versus Boltzmann distribution with "temperature" — $D \approx 0.064$ (magenta curve), grain growth system with mobility of triple junctions $\eta = 100$ and the misorientation parameter $\gamma = 10$. (b) Middle plot, GBCD (red curve) at T_∞ versus Boltzmann distribution with "temperature" — $D \approx 0.058$ (magenta curve), grain growth system with mobility of triple junctions $\eta = 1000$ and the misorientation parameter $\gamma = 100$. (c) Right plot, GBCD (black curve) at T_∞ versus Boltzmann distribution with "temperature" — $D \approx 0.026$ (magenta curve), grain growth system with mobility of triple junctions $\eta \to \infty$ (Herring condition) and the misorientation parameter $\gamma = 1000$.

values of γ and η, give smaller diffusion coefficient/"temperature" — like parameter D for the GBCD at T_∞, and hence higher GBCD peak near misorientation 0. This is in agreement with dissipation–fluctuation relations (2.19), Sec. 2.2.

Next, we consider grain growth systems with different number of grains at initial time T_0, Figs. 10 and 11. Namely, we consider grain growth systems (5.2) with $\mathcal{N} = 1000$, $\mathcal{N} = 2500$, $\mathcal{N} = 10{,}000$ and with $\mathcal{N} = 20{,}000$ grains initially, at time T_0. For these systems, we assume no dynamic misorientation ($\gamma = 0$) and Herring condition

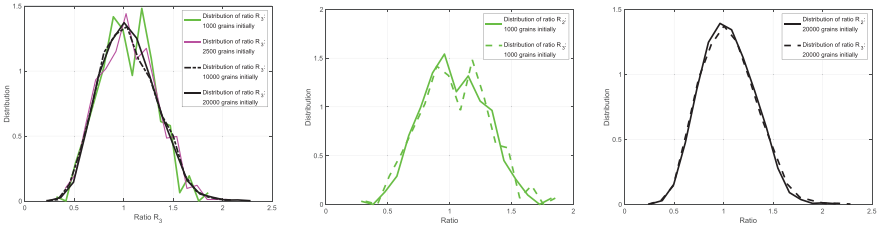

(a) (b) (c)

Fig. 10. (Color online) Grain growth system (5.2) with finite μ (with curvature): (a) Left plot, distributions of ratio R_3 (5.5) system with 1000 grains initially (solid green), system with 2500 grains initially (solid magenta), system with 10,000 grains initially (dashed point black), and system with 20,000 grains initially (solid black). (b) Middle plot, comparison of distributions of ratio R_2 (5.4) (solid green) and R_3 (5.5) (dashed green) for system with 1000 grains initially. (c) *Right plot*, comparison of distributions of ratio R_2 (5.4) (solid black) and R_3 (5.5) (dashed black) system with 20,000 grains initially. Grain growth systems are considered with mobility of triple junctions $\eta \to \infty$ (Herring condition) and no dynamic misorientation ($\gamma = 0$). The closest mesh node of the grain boundary to the triple junction $\boldsymbol{a}$ is used as x_i. The distributions are plotted at T_∞.

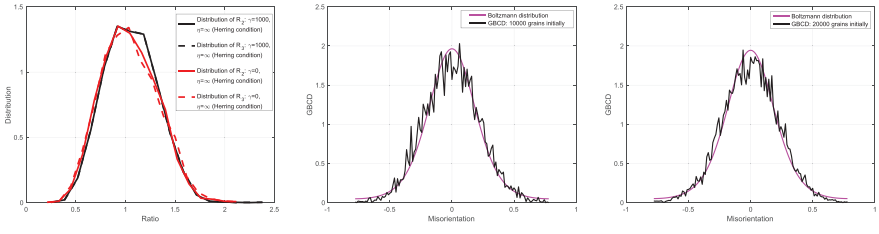

(a) (b) (c)

Fig. 11. (Color online) Grain growth system (5.2) with finite μ (with curvature): (a) Left plot, one run of 2D trial with $10,000$ initial grains, comparison of distributions of ratio R_2 (5.4) (solid black) and R_3 (5.5) (dashed black), grain growth system with mobility of triple junctions $\eta \to \infty$ (Herring condition) and $\gamma = 1000$. Comparison of distributions of ratio R_2 (5.4) (solid red) and R_3 (5.5) (dashed red), grain growth system with mobility of triple junctions $\eta \to \infty$ (Herring condition) and no dynamic misorientations ($\gamma = 0$). The closest mesh node of the grain boundary to the triple junction $\boldsymbol{a}$ is used as x_i. The distributions are plotted at T_∞. (b) Middle plot, one run of 2D trial with $10,000$ initial grains, GBCD (black curve) at T_∞ versus Boltzmann distribution with "temperature" — $D \approx 0.068$ (magenta curve). (c) Right plot, one run of 2D trial with $20,000$ initial grains, GBCD (black curve) at T_∞ versus Boltzmann distribution with "temperature" — $D \approx 0.069$ (magenta curve). Grain growth system with mobility of triple junctions $\eta \to \infty$ (Herring condition) and no dynamic misorientation ($\gamma = 0$).

($\eta \to \infty$) at the triple junctions. From the results, Figs. 10 and 11 (middle and right plots) we observe that distributions for R_2, R_3 and GBCD exhibit convergence to limiting distributions with increase in $\mathcal{N}$. In addition, result on Fig. 11 (left plot), indicates that there is a closer agreement between distributions R_2 and R_3 for larger value of misorientation parameter γ. Again, this is consistent with the developed theory (Sec. 4). In Fig. 12, we investigate effect of the mobility of the triple junctions

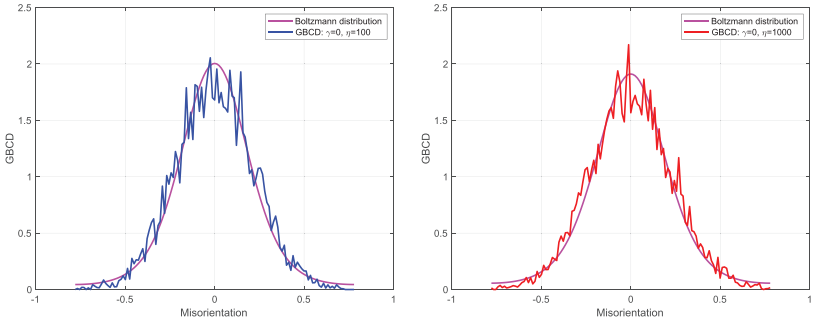

(a) (b)

Fig. 12. (Color online) Grain growth system (5.2) with finite μ (with curvature), one run of 2D trial with 10,000 initial grains: (a) Left plot, GBCD (blue curve) at T_∞ versus Boltzmann distribution with "temperature" — $D \approx 0.066$ (magenta curve), grain growth system with mobility of triple junctions $\eta = 100$ and no dynamic misorientation ($\gamma = 0$). (b) Right plot, GBCD (red curve) at T_∞ versus Boltzmann distribution with "temperature" — $D \approx 0.071$ (magenta curve), grain growth system with mobility of triple junctions $\eta = 1000$ and no dynamic misorientation ($\gamma = 0$).

η on the GBCD, however we do not observe as much effect of η on the GBCD as we observed for the misorientation parameter γ, see Figs. 9 and 12. This can be due to more profound effect of the interactions among triple junctions/correlations effects among triple junctions that should be taken into account as a part of future extension of the proposed stochastic model (2.15).

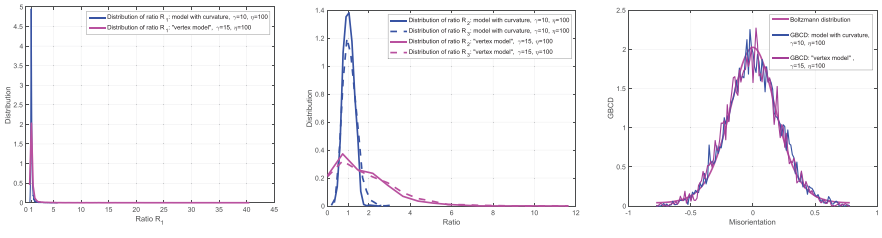

(a) (b) (c)

Fig. 13. (Color online) One run of 2D trial with 10,000 initial grains: (a) Left plot: Comparison of distributions of ratio R_1 (5.3) (solid blue) for model with curvature (finite μ) (5.2) and R_1 (5.3) (solid magenta) "vertex model" with ($\mu \to \infty$) (5.2). (b) Middle plot: comparison of distributions of ratio R_2 (5.4) (solid blue) and R_3 (5.5) (dashed blue) for model with curvature (finite μ) (5.2), and comparison of distributions of ratio R_2 (5.4) (solid magenta) and R_3 (5.5) (dashed magenta) for "vertex model" with ($\mu \to \infty$) (5.2). The closest mesh node of the grain boundary to the triple junction $\boldsymbol{a}$ is used as x_i. The distributions are plotted at T_∞. (c) Right plot: One run of 2D trial with 10,000 initial grains, GBCD (blue curve) "curvature model" (finite μ) (5.2), GBCD (dark magenta curve) "vertex model" ($\mu \to \infty$) (5.2) at T_∞ versus Boltzmann distribution with "temperature" — $D \approx 0.064$ (magenta curve). Grain growth "curvature model" is considered with mobility of triple junctions $\eta = 100$ and $\gamma = 10$, and grain growth "vertex model" is considered with mobility of triple junctions $\eta = 100$ and $\gamma = 15$.

Finally, in the last test, Fig. 13, we compare results of "curvature model" (μ is finite) (5.2) with the results of "vertex model" ($\mu \to \infty$), grain boundaries are straight lines, and hence, only second and third evolution equations of (5.2) are considered for the vertex model, namely model (2.7) which is applied to the grain boundary network is studied. As can be seen from results in Fig. 13, there is not much effect on the GBCD. However, we observe significant effect on the distributions of R_2 and R_3, Fig. 13 (left and middle plots), namely "curvature model" appears to be in closer agreement with the developed stochastic model (2.15) than "vertex model". This again highlights the importance of correlations and their effects on grain growth. Therefore, as a part of future work, we will study interactions/correlations and their effects on coarsening in polycrystalline materials.

6. Conclusion

In this paper, we study a stochastic model for the evolution of planar grain boundary network in order to be able to incorporate and model the effect of the critical events during grain growth (coarsening). We start with a simplified model and, hence, consider the Langevin equation analog of the model from Ref. 21, with the interactions among triple junctions and misorientations modeled as white noise. The proposed system considers anisotropic grain boundary energy which depends on lattice misorientation and takes into account mobility of the triple junctions, as well as independent dynamics of the misorientations. We derive the associated Fokker–Planck equation and establish fluctuation–dissipation principle. Next, due to degeneracy and singularity of the system energy, we use weighted L^2 space to establish long time asymptotics of the solution to the Fokker–Planck equation, the joint probability density function of misorientations and triple junctions, as well as of the closely related marginal probability density of misorientations (the results are obtained under fluctuation–dissipation assumption). As a part of our future work, we will study the logarithmic-Sobolev inequality[1, 2, 27, 42] and construct the L^1 theory of the system.

Furthermore, for an equilibrium configuration of a boundary network, we derive explicit local algebraic relations, a generalized Herring Condition formula, as well as formula that connects grain boundary energy density with the geometry of the grain boundaries that share a triple junction. Even though the considered simplified stochastic model neglects the explicit interactions and correlations among triple junctions, the considered specific form of the noise, under the fluctuation–dissipation assumption, provides partial information about evolution of a grain boundary network, and is consistent with presented results of extensive grain growth simulations. As a part of our future research, we also plan to identify and model explicitly correlations, including nucleation[47, 48] and interactions among triple junctions, as well as extend the theory and mathematical analysis techniques developed in this work to different statistical metrics of grain growth. In addition, we note

that the developed analysis tools can be further adapted to the study of other complementary models of grain growth, e.g. Refs. 46, 50 and 51.

Acknowledgments

The authors are grateful to David Kinderlehrer for the fruitful discussions, inspiration and motivation of the work. The authors are also grateful to colleagues Katayun Barmak and Lajos Horvath for their collaboration and helpful discussions. The work of Yekaterina Epshteyn was partially supported by NSF DMS-1905463 and by NSF DMS-2118172, the work of Masashi Mizuno was partially supported by JSPS KAKENHI Grant No. JP18K13446 and No. JP22K03376, the work of Chun Liu was partially supported by DMS-2118181 and of DMS-2153029.

References

1. A. Arnold, P. Markowich, G. Toscani and A. Unterreiter, On convex Sobolev inequalities and the rate of convergence to equilibrium for Fokker–Planck type equations, *Comm. Partial Differential Equations* **26** (2001) 43–100.
2. D. Bakry and M. Émery, Diffusions hypercontractives, in *Séminaire de Probabilités, XIX, 1983/84*, Lecture Notes in Mathematics, Vol. 1123 (Springer, 1985), pp. 177–206.
3. P. Bardsley, K. Barmak, E. Eggeling, Y. Epshteyn, D. Kinderlehrer and S. Ta'asan, Towards a gradient flow for microstructure, *Atti Accad. Naz. Lincei Cl. Sci. Fis. Mat. Natur.* **28** (2017) 777–805.
4. K. Barmak, A. Dunca, Y. Epshteyn, C. Liu and M. Mizuno, Grain growth and the effect of different time scales, in *Research in Mathematics of Materials Science. Association for Women in Mathematics Series*, vol 31. (Springer, Cham, 2022).
5. K. Barmak, E. Eggeling, M. Emelianenko, Y. Epshteyn, D. Kinderlehrer, R. Sharp and S. Ta'asan, Critical events, entropy, and the grain boundary character distribution, *Phys. Rev. B* **83** (2011) 134117.
6. K. Barmak, E. Eggeling, M. Emelianenko, Y. Epshteyn, D. Kinderlehrer, R. Sharp and S. Ta'asan, An entropy based theory of the grain boundary character distribution, *Discrete Contin. Dyn. Syst.* **30** (2011) 427–454.
7. K. Barmak, E. Eggeling, M. Emelianenko, Y. Epshteyn, D. Kinderlehrer and S. Ta'asan, Geometric growth and character development in large metastable networks, *Rend. Mat. Appl. (7)* **29** (2009) 65–81.
8. K. Barmak, E. Eggeling, D. Kinderlehrer, R. Sharp, S. Ta'asan, A. Rollett and K. Coffey, Grain growth and the puzzle of its stagnation in thin films: The curious tale of a tail and an ear, *Prog. Mater. Sci.* **58** (2013) 987–1055.
9. K. Barmak, M. Emelianenko, D. Golovaty, D. Kinderlehrer and S. Ta'asan, Towards a statistical theory of texture evolution in polycrystals, *SIAM J. Sci. Comput.* **30** (2008) 3150–3169.
10. C. Baruffi, A. Finel, Y. Le Bouar, B. Bacroix and O. U. Salman, Overdamped langevin dynamics simulations of grain boundary motion, *Mater. Theory* **3** (2019) 4.
11. G. Bellettini, *Lecture Notes on Mean Curvature Flow, Barriers and Singular Perturbations*, Appunti. Scuola Normale Superiore di Pisa (Nuova Serie) [Lecture Notes. Scuola Normale Superiore di Pisa (New Series)], Vol. 12 (Edizioni della Normale, 2013).

12. V. L. Berdichevsky, Thermodynamics of microstructure evolution: Grain growth, *Internat. J. Engrg. Sci.* **57** (2012) 50–78.
13. V. Boltyanski, H. Martini and V. Soltan, *Geometric Methods and Optimization Problems*, Combinatorial Optimization, Vol. 4 (Kluwer Academic Publishers, 1999).
14. K. A. Brakke, *The Motion of a Surface by Its Mean Curvature*, Mathematical Notes, Vol. 20 (Princeton Univ. Press, 1978).
15. H. Brezis, *Functional Analysis, Sobolev Spaces and Partial Differential Equations*, Universitext (Springer, 2011).
16. L. Bronsard and F. Reitich, On three-phase boundary motion and the singular limit of a vector-valued Ginzburg–Landau equation, *Arch. Ration. Mech. Anal.* **124** (1993) 355–379.
17. H. B. Callen and T. A. Welton, Irreversibility and generalized noise, *Phys. Rev.* **83** (1951) 34–40.
18. Y. G. Chen, Y. Giga and S. Goto, Uniqueness and existence of viscosity solutions of generalized mean curvature flow equations, *J. Differential Geom.* **33** (1991) 749–786.
19. K. Ecker, *Regularity Theory for Mean Curvature Flow*, Progress in Nonlinear Differential Equations and their Applications, Vol. 57 (Birkhäuser Boston, Inc., 2004).
20. Y. Epshteyn, C. Liu and M. Mizuno, Large time asymptotic behavior of grain boundaries motion with dynamic lattice misorientations and with triple junctions drag, *Commun. Math. Sci.* **19** (2021) 1403–1428.
21. Y. Epshteyn, C. Liu and M. Mizuno, Motion of grain boundaries with dynamic lattice misorientations and with triple junctions drag, *SIAM J. Math. Anal.* **53** (2021) 3072–3097.
22. L. C. Evans, *Partial Differential Equations*, Graduate Studies in Mathematics, Vol. 19 (American Mathematical Society, 1998).
23. L. C. Evans and J. Spruck, Motion of level sets by mean curvature. I, *J. Differential Geom.* **33** (1991) 635–681.
24. Y. Giga, H. Kubo and T. Ozawa, The role of metrics in the theory of partial differential equations, *Hokkaido Univ. Tech. Rep. Ser. Math.* **174** (2018) 1–154.
25. D. Gilbarg and N. S. Trudinger, *Elliptic Partial Differential Equations of Second Order*, Classics in Mathematics (Springer-Verlag, 2001), reprint of the 1998 edition.
26. C. Herring, Surface tension as a motivation for sintering, in *Fundamental Contributions to the Continuum Theory of Evolving Phase Interfaces in Solids* (Springer, 1999), pp. 33–69.
27. A. Jüngel, *Entropy Methods for Diffusive Partial Differential Equations*, SpringerBriefs in Mathematics (Springer, 2016).
28. L. Kim and Y. Tonegawa, On the mean curvature flow of grain boundaries, *Ann. Inst. Fourier* (*Grenoble*) **67** (2017) 43–142.
29. D. Kinderlehrer and C. Liu, Evolution of grain boundaries, *Math. Models Methods Appl. Sci.* **11** (2001) 713–729.
30. J. Klobusicky, Kinetic limits of piecewise deterministic Markov processes and grain boundary coarsening, Ph.D. thesis, Brown Univ. (2014).
31. R. V. Kohn, Irreversibility and the statistics of grain boundaries, *Physics* **4** (2011) 33.
32. R. Kubo, The fluctuation-dissipation theorem, *Rep. Progr. Phys.* **29** (1966) 255–284.
33. O. A. Ladyženskaja, V. A. Solonnikov and N. N. Ural'ceva, *Linear and Quasilinear Equations of Parabolic Type*, Translated from the Russian by S. Smith. Translations of Mathematical Monographs, Vol. 23 (American Mathematical Society, 1967).
34. O. A. Ladyzhenskaya, *The Mathematical Theory of Viscous Incompressible Flow*, Mathematics and its Applications, Vol. 2 (Gordon and Breach, Science Publishers,

1969), Second English edition, revised and enlarged, Translated from the Russian by Richard A. Silverman and John Chu.
35. G. M. Lieberman, *Second Order Parabolic Differential Equations* (World Scientific Publishing Co., Inc., 1996).
36. A. Magni, C. Mantegazza and M. Novaga, Motion by curvature of planar networks, II, *Ann. Sc. Norm. Super. Pisa Cl. Sci. (5)* **15** (2016) 117–144.
37. C. Mantegazza, M. Novaga and A. Pluda, Lectures on curvature flow of networks, in *Contemporary Research in Elliptic PDEs and Related Topics*, Springer INdAM Series, Vol. 33 (Springer, 2019), pp. 369–417.
38. C. Mantegazza, M. Novaga and V. M. Tortorelli, Motion by curvature of planar networks, *Ann. Sc. Norm. Super. Pisa Cl. Sci. (5)* **3** (2004) 235–324.
39. P. A. Markowich and C. Villani, On the trend to equilibrium for the Fokker–Planck equation: An interplay between physics and functional analysis, in *VI Workshop on Partial Differential Equations, Part II (Rio de Janeiro, 1999)*, Vol. 19 (Sociedade Brasileira de Matemática, 2000), pp. 1–29.
40. W. W. Mullins, Two-dimensional motion of idealized grain boundaries, *J. Appl. Phys.* **27** (1956) 900–904.
41. W. W. Mullins, Theory of thermal grooving, *J. Appl. Phys.* **28** (1957) 333–339.
42. F. Otto and C. Villani, Generalization of an inequality by Talagrand and links with the logarithmic Sobolev inequality, *J. Funct. Anal.* **173** (2000) 361–400.
43. R. Temam, *Navier–Stokes Equations*, Studies in Mathematics and its Applications, Vol. 2 (North-Holland Publishing Co., 1979), revised edition, Theory and Numerical Analysis, with an appendix by F. Thomasset.
44. M. Upmanyu, D. Srolovitz, L. Shvindlerman and G. Gottstein, Molecular dynamics simulation of triple junction migration, *Acta Mater.* **50** (2002) 1405–1420.
45. M. Upmanyu, D. J. Srolovitz, L. Shvindlerman and G. Gottstein, Triple junction mobility: A molecular dynamics study, *Interface Sci.* **7** (1999) 307–319.
46. C. Wei, L. Zhang, J. Han, D. J. Srolovitz and Y. Xiang, Grain boundary triple junction dynamics: A continuum disconnection model, *SIAM J. Appl. Math.* **80** (2020) 1101–1122.
47. L. Zhang, L.-Q. Chen and Q. Du, Mathematical and numerical aspects of a phase-field approach to critical nuclei morphology in solids, *J. Sci. Comput.* **37** (2008) 89–102.
48. L. Zhang, L.-Q. Chen and Q. Du, Diffuse-interface approach to predicting morphologies of critical nucleus and equilibrium structure for cubic to tetragonal transformations, *J. Comput. Phys.* **229** (2010) 6574–6584.
49. L. Zhang, J. Han, Y. Xiang and D. J. Srolovitz, Equation of motion for a grain boundary, *Phys. Rev. Lett.* **119** (2017) 246101.
50. L. Zhang and Y. Xiang, Motion of grain boundaries incorporating dislocation structure, *J. Mech. Phys. Solids* **117** (2018) 157–178.
51. Q. Zhao, W. Jiang, D. J. Srolovitz and W. Bao, Triple junction drag effects during topological changes in the evolution of polycrystalline microstructures, *Acta Mater.* **128** (2017) 345–350.